5-5-2012

Nanocharacterization of Porous Materials with Atomic Force Microscopy

Yasemin Kutes
Institute of Materials Science, yaseminkutes@gmail.com

Nanocharacterization of Porous Materials with Atomic Force Microscopy

Yasemin Kutes

B.S. Middle East Technical University, 2009

A Thesis

Submitted in Partial Fulfillment of the

Requirements for the Degree of

Master of Science

at the

University of Connecticut

2012

APPROVAL PAGE

Master of Science Thesis

Nanocharacterization of Porous Materials with Atomic Force Microscopy

Presented by

Yasemin Kutes, B.S.

Major Advisor _____
Bryan D. Huey

Associate Advisor _____
Mei Wei

Associate Advisor _____
Yusuf Khan

University of Connecticut

2012

Acknowledgements

First, I would like to thank my advisor Dr. Bryan D. Huey for his encouragement and guidance throughout this work and also for his understanding and support through hard times. I would also like to thank Huey nmLab members; Dr. Varun Vyas, Vincent Palumbo, Linghan Ye, James Louis Bosse, Alejandro Lluberes, Joshua Leveillee for their help and support in my efforts and creating a friendly work environment.

I would also like to thank the workers at Asylum Research for providing readily available technical support for the AFM and especially for "iDrive".

I would also like to mention Dr. George Rossetti for letting me work in his lab and his students for their help.

Finally, I would like to thank my family in Turkey for the endless love and support they send from thousands of miles away.

This thesis is dedicated to my late uncle, Mehmet Kutes.

Table of Contents

List of Figures

Abstract

Scanning Probe Microscopy techniques have proven very useful in the investigation of porous nanostructured surfaces. Especially, Atomic Force Microscopy (AFM) has been widely used due to its compatibility with non-conducting surfaces. In particular, AFM often complements other techniques like scanning and transmission electron microscopy by providing quantitative surface information coupled with nanoscale spatial resolution. Its ability to operate in fluid is also important, as this allows researchers to mimic the physiological environment of biological materials and systems. In this work, two main types of porous materials are studied with AFM, including Phosphoric Acid Fuel Cell (PAFC) electrode catalyst layers, and human molar dentin. Although these systems apply to very different areas of materials science, there are many commonalities in terms of feature sizes, surface morphology, and appropriate imaging methods.

The contribution of electrocatalyst layer microstructure to the performance of gas diffusion electrodes in PAFC's is extremely important. These structures contain different levels of porosity and particles ranging from several nanometers to several micrometers, along with 1-10 nanometers thick coating materials. Therefore, characterization of these surfaces is crucial to understanding the mechanisms affecting fuel cell efficiencies. Similarly, the human molar dentin layer, crucial in restorative dentistry, comprises features ranging from 70 nm (collagen bands) to 4um (tubules). This biological material can be studied in vitro with AFM, retaining its properties and resulting in more realistic results.

In the work presented in this thesis, AC mode AFM imaging (both in-air and in-liquid) was utilized to probe nanoporous surfaces of PAFC catalyst layers and human dentin.

For in-air AC imaging of electrocatalyst layers, a piezo-actuated cantilever with a super sharp tip attached to it is oscillated in its resonant frequency to raster scan over the surface of the material. With this technique the amount of time the AFM tip spends on the material is minimized, thereby limiting damage to the specimen and tip. Height and Phase data are collected in order to investigate the topographical and physical characteristics of the material with and without phosphoric acid (PA) loading. Results show that catalyst particles less than 100nm in diameter are resolvable with AFM, and PTFE coating seems to be incomplete in some cases. PTFE separation form catalytic particles in the PA loaded cathode are detected. PA loading seems to significantly increase the phase contrast.

For in-liquid AC imaging of human dentin samples, a very soft cantilever is electro-magnetically oscillated to more gently and reliably image the collagen and carbonated hydroxyapatite surface. The surface morphology is then monitored upon deposition of a polymeric solution using a spin coater. The properties of bare and coated surfaces are compared, and the development of the coating morphology for a single layer, as well as for sequential layers, was investigated. Results indicate that multiple polymer layers smooth the surface significantly, masking nanometer scale features such as collagen bands. In some cases dentinal tubules, approximately 4 um in diameter, are also occluded in the process. This is true in air, and in vitro, mimicking the conditions in the human mouth.

Chapter 1: Introduction

1.1Overview

It is crucial to study materials mimicking their appropriate environment with a nondestructive characterization tool without inducing changes to the actual structure. Atomic force microscopy (AFM) is a member of the larger scanning probe microscopes family which uniquely can operate in relevant conditions permitting quantitative, high resolution imaging.

In the work presented in this thesis, AC mode AFM imaging (both in-air and in-liquid) was utilized to probe nanoporous surfaces of phosphoric acid fuel cell (PAFC) catalyst layers and human dentin. Both materials require the appropriate imaging environment fully or partially relating to their operating or physiological conditions.

PAFC catalyst layers are composed of Platinum catalyst particles which accelerate oxygen reduction reactions. To reduce the amount of precious metal used, platinum is usually supported on carbon in the form of nano-dispersed particles. This dispersement allows for high-catalyst surface areas at low-catalyst loadings. Carbon supported catalysts are, however, susceptible to catalyst particle agglomeration. Another major drawback is the corrosion of carbon support which leads to performance decrease due to accelerated loss of active surface area [1], alteration of pore morphology, and pore surface characteristics [2]. Carbon corrosion may also arise from the removal of water-repelling agents (usually PTFE coating) upon phosphoric acid loading of the electrodes under high pressure, which especially poses problems to the cathode layer. Pt particle distribution

and size may successfully be monitored utilizing in–air AFM imaging. Also AFM may uniquely enable the identification of PTFE separation from the catalyst and/or carbon support particles.

Human dentin is a vital hydrated tissue. It is strongly sensitive to dehydration and drying that are commonly used in preparation of samples in examinations by techniques like electron microscopy. Its ultrastructure and properties are used as the basis for most of the operations in restorative dentistry; hence its characterization in its physiological environment is crucial. AFM can be operated in a fluid chamber, which may successfully mimic the conditions in a human mouth, allowing restorative coatings on teeth to be more relevantly investigated.

1.2Scanning Probe Microscopy (SPM) on Porous Nanostructured Surfaces

SPM and especially the two primary variations; scanning tunneling microscopy (STM) and atomic force microscopy (AFM), are being used for studying porous surfaces due to the nanoscale resolution capabilities. AFM, which was invented a few years later than STM, has become particularly widespread as it is compatible with non-conducting materials.

Two main elements [3] are responsible for the high resolution capability of these instruments; namely a very sharp tip probing the surface of interest, and a piezoceramic scanner controlling the tip position with very high precision. This has allowed researchers to obtain down to atomic resolution for atomically flat and highly crystalline surfaces [4].

As the application area of SPM expands, it was realized that these instruments are well suited to studying porous surfaces to complement other techniques like scanning and transmission electron microscopes [5]. The primary restrictions are that SPM only probes the outermost surface of the sample since it is essentially a contact or near contact technique. Related to this, the finite dimensions of the probing tip limit the size of the pores detectable. Especially, any pore significantly smaller than the tip evidently cannot be resolved, since the tip simply cannot get into such a small pore. Surfaces with high roughness are also inherently challenging with SPM, though this can be mitigated with quality equipment and training.

An important advance in SPM and especially micro manufacturing is the development of consumable SPM probes with a wide spectrum of characteristics. Ultra sharp tips such as carbon nanotubes attached to AFM probes have diameters of only a couple of nanometers, alleviating some of the limitations caused by standard tip dimensions for porous materials investigations. Compared to regular probes with apex diameters that are tens of nanometers across, ultra sharp probes can provide detailed data in the 2-50 nm range.

For example, in the first known studies by AFM of activated carbon cloths and fibers, Brasquet et al. [6, 7] failed to attain a resolution in the micropore range, utilizing a tip with 30 nm radius of curvature. However; they observed features such as veins which did not appear in SEM images, inclined from 45 to 90 degrees towards the fiber axis, and from 10 to 40 nm in size. Figure 1 shows an SEM and an AFM image of such fibers, and the previously unresolved venous structures, respectively. The results obtained from SEM and AFM otherwise compared very well, accentuating the advantages of AFM over SEM

in providing precise and quantitative local information about surface topography. Of course for large areas electron microscopy has significant advantages in terms of imaging speed, but when topographic and especially features with heights or depths on the order of nanometers are important, AFM is a crucial tool.

(a) 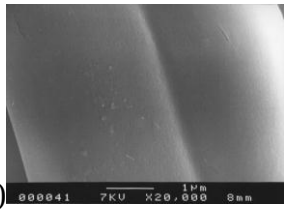 (b) 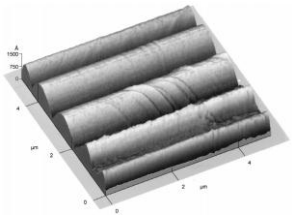

Figure 1. (a) SEM image of fibers (b) AFM image of fibers [7]

Another study where AFM was used to visualize porous structures was on oxide-based materials. Studying vanadia-silica glasses, Curran et al. [8] were able to explain the increased microporosity when vanadium was incorporated to the silica xerogel. They found that materials with vanadium concentration as low as 0.01 mol % are more microporous than pure silica samples. The reason was revealed by AFM imaging which showed filling of mesopore regions in the materials containing vanadium.

AFM has also been used to investigate the pore structure of microfiltration membranes of different materials and pore sizes. Bowen et al. [9] was able to obtain very high resolution images of membranes from which they derived statistical data such as pore size, density and distribution. Another AFM study was conducted by Bailey et al. [10] on alumina microfiltration membranes where different precursors were used to prepare the

material to be characterized. Results of this study, where tapping mode AFM was used, indicate that pore morphology changes as the precursors change.

Organic and biological materials have been studied by AFM as well in terms of pore morphologies. Stamatialis et al. [11] studied a series of cellulose ester membranes of which they obtained images of surface morphology. They reported the surface morphology in terms of various roughness parameters such as mean roughness, z-range or root mean square of z values. They concluded that permeation properties of these membranes (NaCl rejection) were improved with decrease in surface roughness as measured by AFM.

Hennesthal et al. [12] studied suspended bilayers, a class of artificial membrane systems, which are based on lipid bilayers supported on porous alumina. Comparison of AFM and SEM images showed that tip-sample convolution effects took place in AFM scanning of alumina support. It was reported that pore size appears to decrease to an average diameter of 50±10 nm in AFM images compared to the pores in SEM images which average to 60±10 nm. AFM (1um x 1um) and SEM images can be seen in Figure 2.

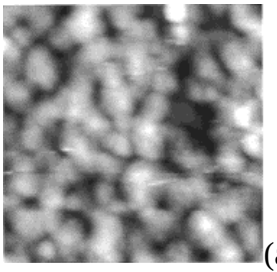
(a)

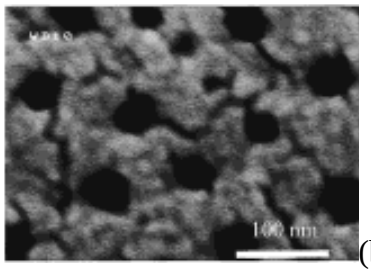
(b)

Figure 2. (a) 1 um^2 AFM image of alumina membrane, (b) SEM image of alumina membrane [13]

Human molar dentin structure was studied by Zapletalova et al. [13] by AFM under moist conditions. Some biological tissues such as dentin contain a high amount of water and organic matter and are very sensitive to dehydration. In this study, samples were stored in distilled water and imaged with AFM under moist conditions whereas in SEM imaging, the samples had to be dehydrated in graded acetone series, dried and coated in sputtering device after fixation. It is reported that artifacts caused by shrinking occurred.

1.3Fuel Cell Electrodes

"Fuel cells (Figure 3) are electrochemical devices that convert the chemical energy of a reaction directly into electrical energy" [14]. Efficiency of fuel cells is higher and they are less noisy and cleaner than conventional technologies since no combustion occurs in the process. They can produce electricity continuously as long as the necessary fuel and oxidant are supplied; they do not need to be recharged.

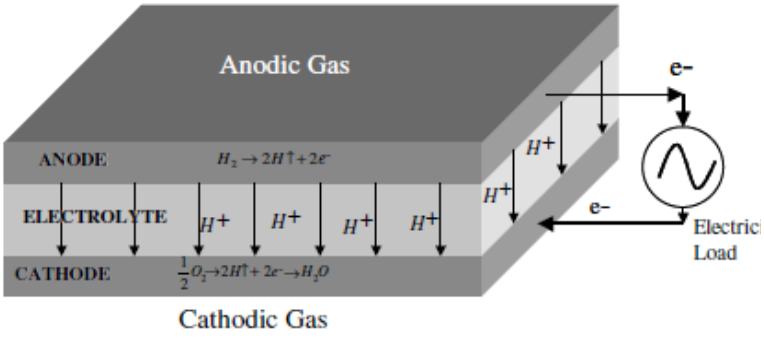

Figure 3. Simplified Fuel Cell Schematic [15]

"The components of a fuel cell are anode, anodic catalyst layer, electrolyte, cathodic catalyst layer, cathode, bipolar plates/interconnects and sometimes gaskets for sealing/preventing leakage of gases between anode and cathode" [16]. The anode and cathode are composed of permeable gas diffusion layers usually made of materials with high electron conductivity such as porous graphite thin layers. One of the most common catalysts is Platinum (Pt) for low temperature fuel cells and Nickel (Ni) for high temperature fuel cells. The electrolyte material should provide high proton conductivity and theoretically zero electron conductivity. Interconnects or in other words; bipolar plates are responsible for collecting electrical current and distribution of reactive gases in the fuel cell stack.

There are two main technical problems with fuel cells which are the slow reaction rate causing low currents and power, and the fact that hydrogen as a fuel is not readily available. Many different fuel cell types have been developed addressing these problems. These different fuel cell types are generally categorized by their electrolyte type although they hold other major differences as well. Feasible for the present and near future, there are six fuel cell types, namely; proton exchange membrane (PEM) fuel cell, alkaline fuel cell (AFC), direct methanol fuel cell (DMFC), ***phosphoric acid fuel cell (PAFC)***, molten carbonate fuel cell (MCFC) and solid oxide fuel cell (SOFC).

In this work, we are specifically interested in ***phosphoric acid fuel cell (PAFC) electrodes***. "PAFC is the most mature of all hydrogen fuel cell systems and is the only fuel cell technology that is in commercialization" [17]. 150-190˚C and ambient to 5 atm are its operating temperature and pressure ranges respectively. This temperature range

allows PAFC to take up hydrogen directly from hydrogen sources like reformer gases. Other elements of PAFC are mainly carbon and graphite [17].

In a fuel cell, the electrolyte material has three important functions. It transports dissolved reactants to the electrode and carry ionic charge between the electrodes completing the cell circuit. It also provides a physical barrier to prevent the fuel and oxidant gas streams from directly mixing [14]. "Phosphoric acid (H_3PO_4) is the only common inorganic acid that has enough thermal stability, chemical, and electrochemical stability, and low enough volatility (above about 150˚C) to be considered as an electrolyte for fuel cells" [18]. Most importantly, phosphoric acid is tolerant to CO_2 in the fuel and oxidant. It was therefore chosen by the American company, United Technologies (later the spin-off ONSI Corporation), back in the 1970s as the preferred electrolyte for terrestrial fuel cell power plants [18].

A PAFC is composed of two porous gas diffusion electrodes; namely anode and cathode, Figure 4. Anode, electrolyte layer and cathode are set side by side. The gas diffusion electrodes are permeable substrates fed with gas. The substrate is a porous carbon paper/cloth. On the other side of this substrate which faces the electrolyte (phosphoric acid), platinized fine carbon powder electrocatalyst is roll coated with polytetrafluoroethylene (PTFE) as a binder.

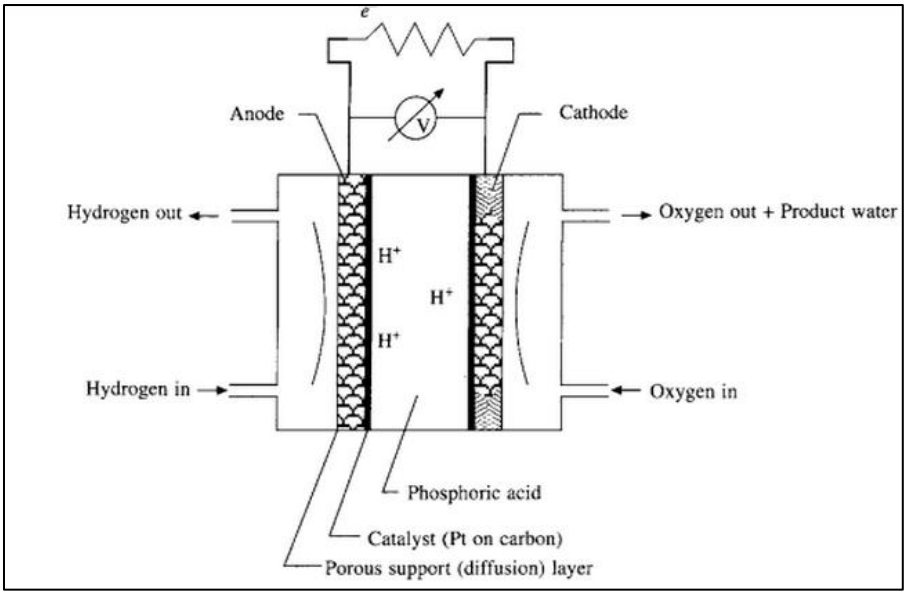

Figure 4. Components of PAFC [17]

Porous electrodes in fuel cells are home to gas/liquid ionization or de-ionization reactions, they conduct ions away from or into the three phase interface once they are formed, and they also act as a physical barrier that separates the gas phase and the electrolyte. In order to increase the rates of reactions, the electrode material should be catalytic, conductive and porous. The catalytic quality of electrodes especially becomes important in lower temperature fuel cells since ionization reaction rates increase with temperature. Another concern is that these electrodes must be permeable to both electrolyte and gases, but not such that the media can easily be "flooded" by the electrolyte or "dried" by the gases on one side [14]. PTFE binder for example, in phosphoric acid fuel cells act as a hydrophobic layer preventing the flooding of pores.

The porous electrodes used in PAFCs are described extensively in Kinoshita's book [19]. These electrodes contain a mixture of the electrocatalyst supported on carbon black and a polymeric binder, usually PTFE (about 30 to 50 wt %). The carbon black particles are bound together by PTFE forming a through but porous structure, which is supported on a porous carbon paper substrate. "The carbon paper serves as a structural support for the electrocatalyst layer, as well as the current collector. A typical carbon paper used in PAFCs has an initial porosity of about 90%, which is reduced to about 60% by impregnation with 40 wt % PTFE" [19]. This carbon paper contains pores of diameter ranging from 3 to 50 um (median pore diameter of about 12.5 um) and micropores with a median pore diameter of about 34 Å for gas permeability. A simple view of these structures can be seen in Figure 5.

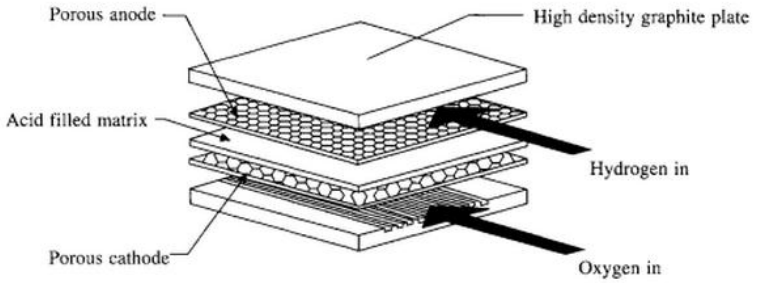

Figure 5. Exploded view of PAFC [17]

Carbon black agglomerates embody small primary particles, 0.02-0.04 um, which become ca. 0.3 um in size when mixed with PTFE. PTFE may not cover the surface of carbon black thoroughly, because of the large size of PTFE particles. "The space in the agglomerates or that between the agglomerates and PTFE may act as gas networks at the initial stage of operation, but fill with electrolyte eventually because of the small contact

angle of carbon black, uncovered with PTFE, to electrolyte (<90˚), resulting in the degradation of cell performance" [14]. Increasing the PTFE content has not helped to solve this issue because it causes a decrease in catalyst use.

The contribution of electrocatalyst layer microstructure to the performance of gas diffusion electrode in a PAFC is thus extremely important. Most of the structural characterization studies have been done using electron microscopes and quantitative data was obtained by other means such as porosimetry or modeling. Choi et al. [20] investigated the shape and microstructural evolution with temperature of PTFE in the electrocatalyst layer made of various Pt-C composites. They observed the fractured surface of small pieces of electrodes with SEM. The porosity and pore size distribution of the electrocatalyst layer was determined by a mercury porosimeter. Interestingly, they noted the presence of Teflon fibrils in the electrodes, which they were able to conclude, were not formed during the fabrication process but rather were present as a raw material component of the initial PTFE supply, see Figure 6. They observed that PTFE was present as particles and fibrils before sintering and clusters were transformed to a cluster or honeycomb shape network of thin films or filaments after sintering.

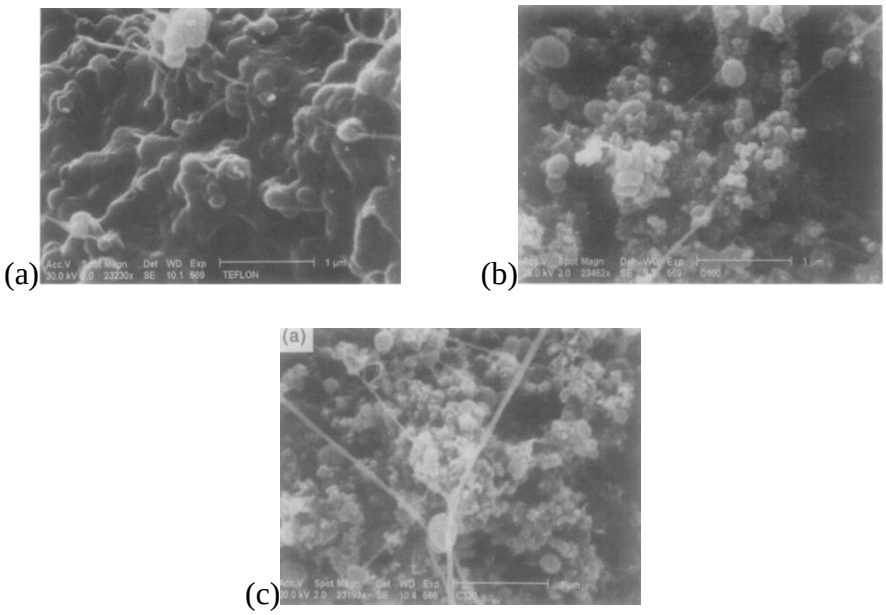

Figure 6. SEM micrographs of (a) Bulk PTFE (b) Catalyst layer after rolling process (c) PTFE in the form of particles and fibers in the catalyst layer [20]

1.4Tooth Anatomy and Dentin Microstructure

Each tooth has two parts; crown and root. Crown and root are covered with enamel and cementum, respectively. The crown and root join at the cementum-enamel junction called the cervical line, see Figure 7.

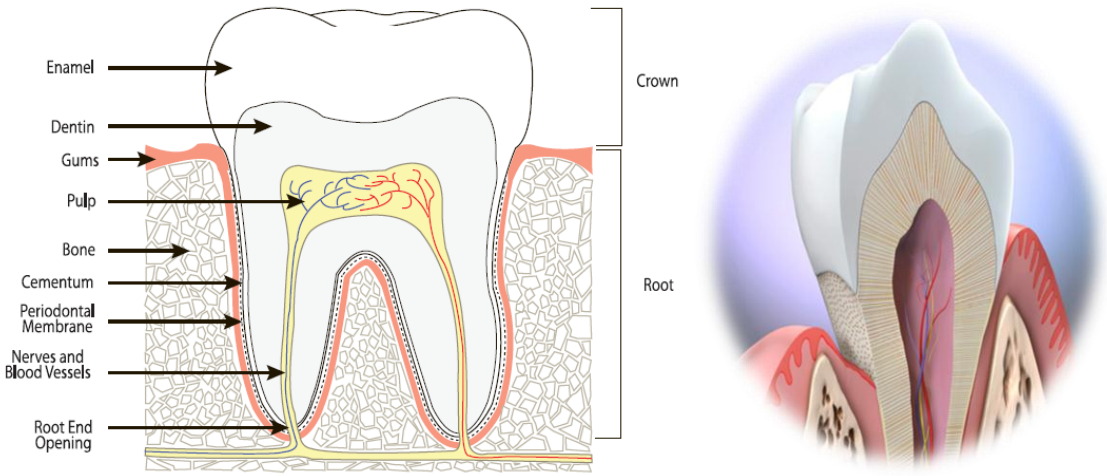

Figure 7. Tooth Anatomy (www.oralhealth.ncdhhs.gov)

In the crown portion, teeth consist of three layers; enamel, dentin and the pulp from outside to inside respectively. The dentin and the pulp of the crown also extend into the root where there is no enamel coating. The pulp is known as pulp chamber in the crown and pulp canal in the root. The pulp chamber and pulp canal are collectively known as the pulp cavity [21].

In this study, we are primarily interested in the dentin layer of human molar teeth. Dentin is a vital, hydrated composite material with structural components and properties that vary with location [22]. "Primary dentin is formed during tooth development. Its volume and conformation, reflecting tooth form, vary with the size and shape of the tooth. Dentin is composed of about 50 vol % mineral in the form of a carbonate rich, calcium deficient apatite; 30 vol % organic matter which is largely type I collagen; and about 20 vol % fluid, which is similar to plasma but is in fact poorly characterized" [23]. The rest of the volume, which is very small, is composed of other non-collagenous proteins and other organic components, functions of which are not very well established. The major components are distributed into distinctive morphological features to form a vital and complex hydrated composite in which the morphology varies with location and undergoes alterations with age or disease [24].

Particularly interesting for this study are the tubules, distinct and important features of dentin, representing the path odontoblastic cells follow from the dentin-enamel junction (DEJ) or cementum (outer layers) to the pulp chamber (tooth core). Tubules converge on the pulp chamber which results in varying tubule orientations and densities from location to location (Figure 8). Number of tubules is lowest at the DEJ and highest at the

predentin surface at the junction to the pulp chamber. Odontoblast processes take place on all or part of a tubule's course. The tubule lumen is mostly lined with peritubular dentin (also termed as intratubular dentin) which is highly crystallized (apatite) with little organic matrix [22]. The tubules are further separated by intertubular dentin composed of a matrix of type I collagen reinforced by apatite. The amount of this intertubular dentin varies with location as well, equivalent to the density of tubules changing with position and depth [22]. Both enamel and dentin include apatite; however dentin apatite has a much smaller crystallite size, higher carbonate content and higher susceptibility to acidic dissolution than enamel apatite.

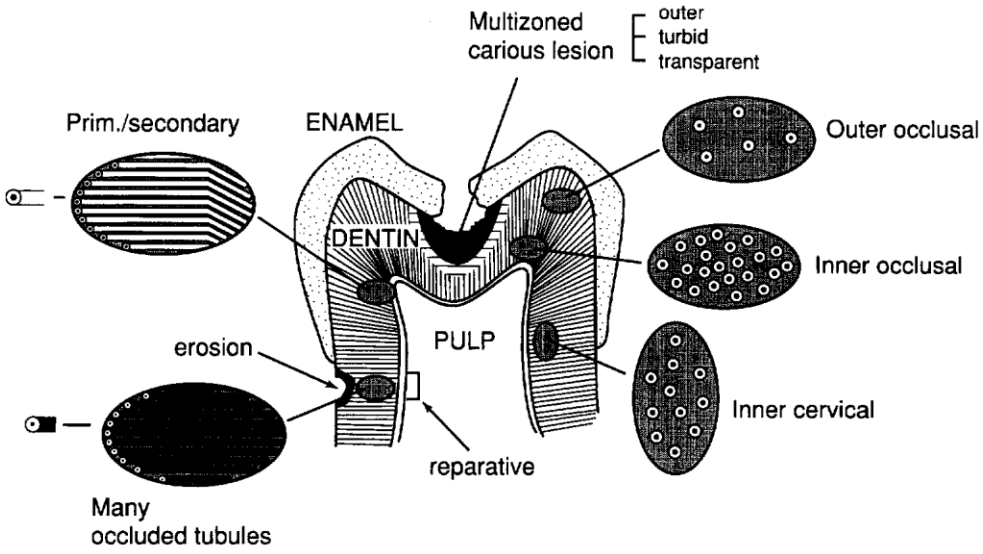

Figure 8. Schematic diagram of dentin structural variations with intratooth location, formation of secondary dentin and several altered forms of dentin due to occlusal caries and and cervical sclerosis [22]

Dentin microstructure and properties are the most important basis of nearly all operations in restorative dentistry. Hence, substantial research has been conducted for the characterization of dentin layers in terms of dentin bonding, mechanical property

distributions, de/remineralization of intertubular dentin, and even distributions of piezoelectric properties. Since the ultrastructure of dentin consists of components on the order of microns and nanometers, studying these surfaces with nanocharacterization tools such as atomic force microscopy (AFM) is crucial. Figure 9 shows further areas of use for AFM in dentistry research to quantitatively probe various natural and artificial dental surfaces and structures [25].

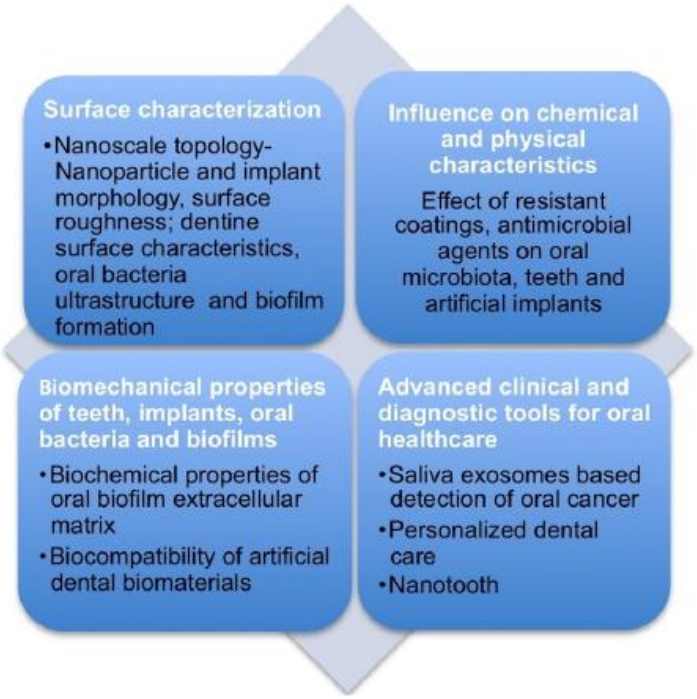

Figure 9. AFM based nanoscale topographic, biophysical and biochemical characteristics of dental surfaces and structures [25]

AFM is also very suitable for studying the collagen structure and dentin surface changes caused by different chemicals since it requires minimal sample modification and alteration before and during scanning, unlike scanning electron microscopy (SEM) which

requires a certain degree of sample electrical conductivity, gold or carbon coating and works in a vacuum environment.

Silikas et al. [26] studied the morphology and roughness of human dentin surfaces after treating with different agetns with tapping mode AFM imaging. They followed a sequential imaging method. That is, “each surface was examined after the treatment with SiC paper, with the smear-layer present, and then re-examined after conditioning treatment. In this way, each specimen was used as its own reference” [26]. SEM does not allow such a treatment. They used 4 different types of conditioners; namely phosphoric acid, and 3 commercial products, all common in professional dentistry [26]. The authors call attention to the fact that a vast number of conditioning agents are available on the market, but their effectiveness is less than clear, motivating such topographic studies of the influence of these agents.

The results obtained by Silikas et al. suggest that the entire surface morphology and roughness showed variations, but to a degree that depended on the conditioning agent used (Figure 10). They suggest that these differences might affect the bonding properties of other agents in dentin/polymer systems such as cement/epoxy, resin composites or other polymeric restorative agents.

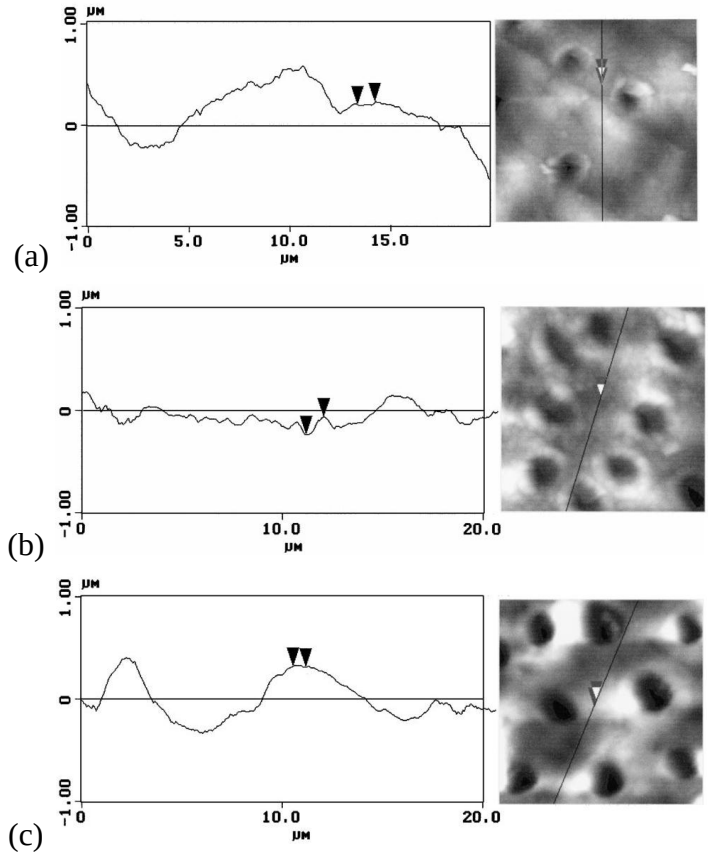

Figure 10. (a) Dentin surface profile (left) of a typical area between the tubules of a 15s phosphoric acid etched sample. Note the local variation in height (measured between the arrows in the profile) of about 30 nm. (b) Dentin surface profile (left) of a typical area between the tubules of a 30s Panavia21 treated sample. Note the local variation in height (measured between the arrows in the profile) of about 170 nm. (c) Dentin surface profile (left) of a typical area between the tubules of a 30 s Scotchbond MP treated sample. Note the local variation in height (measured between the arrows in the profile) of about 10 nm. [26]

Bertassoni et al. [27] studied structural and mechanical changes leading to reminaralization of dentin to understand the conditions under which this mineral binds with a demineralized dentin matrix (flaw in a tooth) in order to achieve surface mechanical recovery. They used AFM nanoindentation to determine the degree of mechanical hardness, and hence mineralization, on the surface as compared to unrecovered specimen regions. Indentations were made with the specimens placed in a fluid cell filled with water, and employed a calibrated Berkovich diamond indenter on an atomic force microscope (AFM; Nanoscope III Digital Instruments, Santa Barbara, CA)

with the standard head replaced by a Triboscope indenter system to obtain values of reduced elastic modulus (E). [27]

Nanoindentation performed by AFM is very accurate in positioning the tip on intertubular region or on peritubular dentin, bypassing the tubules. They used AFM topography imaging to characterize the changes occurred in surface morphology. Imaging was performed in the contact mode in air using a silicon tip at a scan speed of 0.5-1 Hz. [27]. They quoted "Although we attempted to obtain images in water for this study, we had difficulties in obtaining high-quality and interpretable data, therefore images shown are from the samples after drying under ambient conditions." [27]

AFM images (Figure 11) revealed the slightly elevated (lighter region) peritubular dentin surrounding each tubule lumen, whereas the slightly lower (darker region) intertubular region showed evidence of the collagen network as indicated by the slight variations in topography. [27]

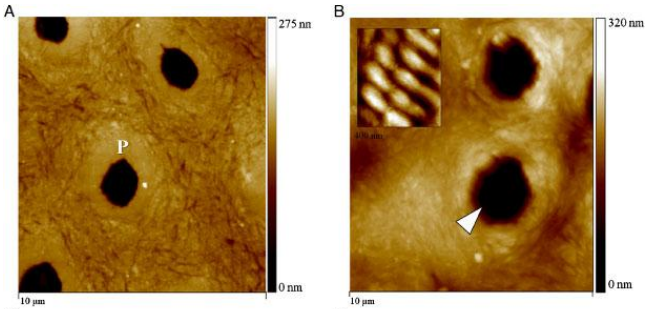

Figure 11. (A) 10 um AFM scan of normal dentin showing peritubular mineral surrounding tubules; (B) demineralized dentin exhibited surface roughened topography and widened tubular lumens (arrowhead) Fully demineralized collagen from dentin is shown in the detail for comparison purposes (400 nm scan). [27]

Wallace et al. [28] quoted “AFM is a convenient way to study collagen structure in various tissues because it provides accurate quantitative measurements with the least disruption to the tissue which remains intact to a great extent, decreasing the possibility of artifacts.” They studied the distribution of type I collagen in hard tissues like teeth, bone and tendons. They imaged samples in air using a PicoPlus 5500 AFM (Agilent). Dentin and bone were imaged in tapping mode using silicon cantilevers (VistaProbes T300R, tip radius<10nm, force constant 40 N/m, resonance frequency 300 kHz; nanoScience Instruments; Phoneix, AZ). Images were acquired from 3 locations in each of 5 teeth; at each location, amplitude or deflection images 3.5 um on a side were analyzed to investigate the D-periodic spacing of the collagen (Figure 12).

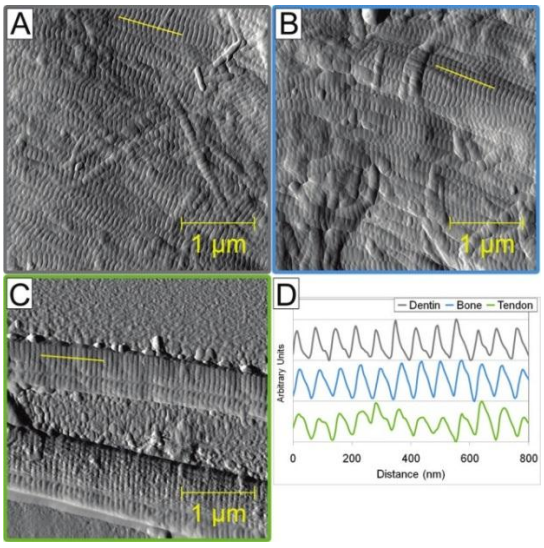

Figure 12. Representative line scans from each tissue. This figure shows representative 3.5 um x 3.5 um amplitude images from dentin (A) and bone (B), and a deflection image from tendon (C). The yellow line in each panel is where a representative line scan was performed (D). The line scans in panel D are shown on a normalized height scale for comparison purposes. [28]

1.5Dentin Hypersensitivity

Dentin hypersensitivity can be described as very short term, sharp pain due to exposed dentin (particularly exposed tubule channels). The dentin layer of the tooth can get exposed as a result of enamel loss on the tooth crown, or gum recession on the root of the tooth. Enamel can be lost due to over aggressive or incorrect tooth brushing, highly acidic dietary consumption or tooth grinding caused by stress and parafunctional behavior. Gum recession, on the other hand, might also occur as a result of incorrect brushing as well as some dental surgical procedures. Once the root gets exposed to the oral cavity, the outer cementum layer can be removed very easily, exposing dentin tubules [29].

Researchers have come up with many theories to clarify the mechanism of dentin hypersensitivity [30]. Of these the most widely accepted one is the so-called hydrodynamic theory of sensitivity (Figure 13). This theory proposes that quick shifts of the dentinal fluid, in either direction, following an applied stimulus, result in activation of sensory nerves in the pulp/inner dentin region of the tooth [3, 31]. The hydrodynamic hypothesis for dentin sensitivity was proposed a hundred years ago [3] with confirming evidence published in the 1950s and 1960s [31]. Hydrodynamic flow can be increased by changes in temperature, humidity, air pressure and osmotic pressure, or forces acting on the tooth. Hot or cold foods and drinks, and physical pressure are typical triggers in people with dentin hypersensitivity [29]. Berman [32] quotes "The coefficient of thermal expansion of the tubule fluid is about ten times that of the tubule wall. Therefore, heat applied to dentin will result in expansion of the fluid and cold will result in contraction of the fluid, both creating an excitation of the 'mechanoreceptor' nerves.

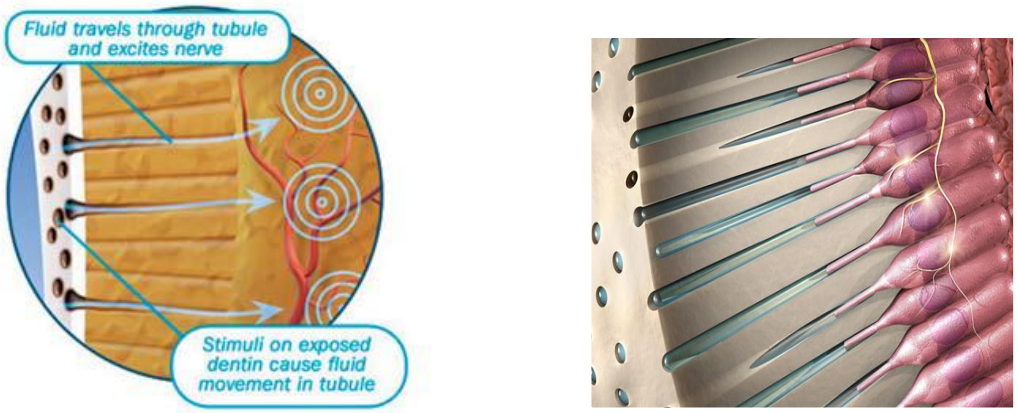

Figure 13. Depiction of Brannstrom's [31] Hydrodynamic Theory [33]

Treatments for dentin hypersensitivity can be grouped as invasive or noninvasive. Invasive procedures may include gingival surgery, resin application or application of lasers. Non-invasive treatment options are topical agents and dentifrices that contain a desensitizing active ingredient which are obviously, much simpler and more cost-effective for most patients. Some of the topical agents include active ingredients such as potassium ions which block the synapses between nerve cells, decreasing nerve sensitivity and hence the resulting pain. Other treatments are designed to reduce flow into the dentin tubules by occluding the tubules [33].

Topical desensitizing agents have been classified [34] on the basis of their chemical and physical properties as follows:

Chemical agents: Corticosteroids, silver nitrate, strontium chloride, formaldehyde, calcium hydroxide, potassium nitrate, fluorides, sodium citrate, potassium oxalate, iontophoresis with 2% sodium fluoride

Physical agents: Composites, resins, varnishes, sealants, soft tissue grafts, glass-ionomer cements, lasers

In 1935, Grossman described an ideal desensitizing agent as follows: “The ideal desensitizing agent should not irritate or endanger the integrity of the pulp, should be relatively painless on application or shortly afterward, should be easily applied, rapid in action, permanently effective and finally should not discolor tooth structure [35]. “To date no such treatment has been discovered and there is no ‘gold standard’ by which to assess new treatments” [36].

1.6Influence of Tubules on Dentin Hypersensitivity

Petrou et al. [37] worked on a breakthrough therapy for dentin hypersensitivity, which is now widely accepted to explain the mechanism and is described separately in Section 1.5 [38]. Fluid movement within the microtubules caused by external stimuli such as heat, cold, evaporation, or pressure changes results in sharp pain responses in the nerves at the bottom of the tubule channels [39]. There are two main approaches in treating this hypersensitivity; to inhibit nerve transmission, or to occlude the dentin tubules.

There are several ways to achieve such dentin tubule occlusion which range from invasive techniques, such as laser etching of the dentin surface [40], to noninvasive methods such as the application of a gel or toothpaste containing an occluding agent [41].

In their work, Petrou et al. used a product containing arginine and calcium carbonate to occlude dentinal tubules. AFM was used to evaluate dentin surfaces before and after treatment with the prophylaxis paste containing 8% arginine and calcium carbonate. Untreated dentin was used as a control (Figure 14).

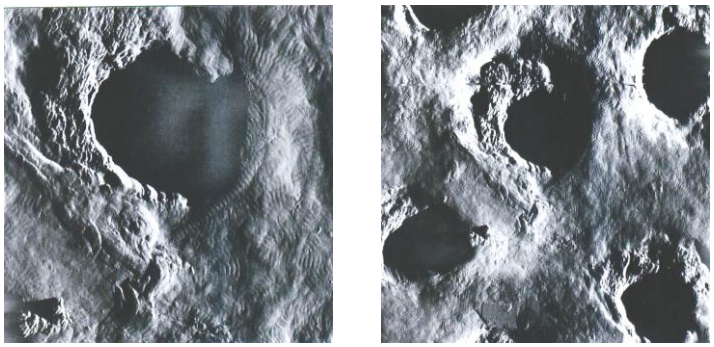

Figure 14. Untreated dentin – single tubule (left), multiple tubules (right) [37]

The AFM images of untreated dentin show that the tubules were completely open. Zooming in on a single tubule reveals a helical fine structure on the dentin surface (collagen as noted above). The AFM images of a treated specimen (Figure 15) show that these collagen structures were no longer visible, as a result of formation of a protective layer. Furthermore, the tubules were sealed shut.

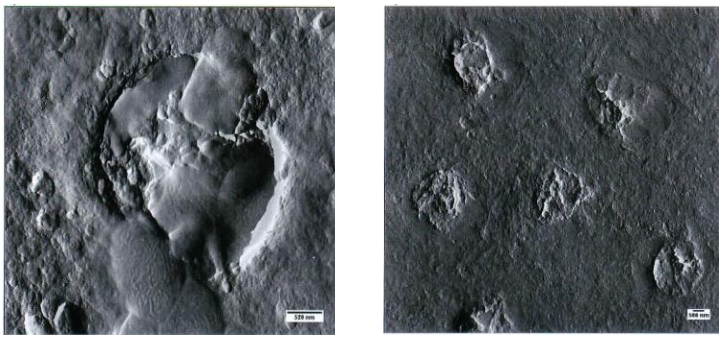

Figure 15. AFM images of dentin treated with the desensitizing prophylaxis paste containing 8% arginine and calcium carbonate – single tubule (left), multiple tubules (right) [37]

Kubinek et al. [42] studied dentin structures of extracted human third molars by SEM and AFM, see Figure 16. They used contact mode AFM imaging in a liquid environment to avoid artifacts due to dehydration of the samples. An AFM Explorer manufactured by Veeco-ThermoMicroscopes (USA) was applied using contact mode with tips from silicon nitride (type 1520-00, Veeco). The scan size varied from 5 to 100 µm and a resolution of 300 points per row was used.

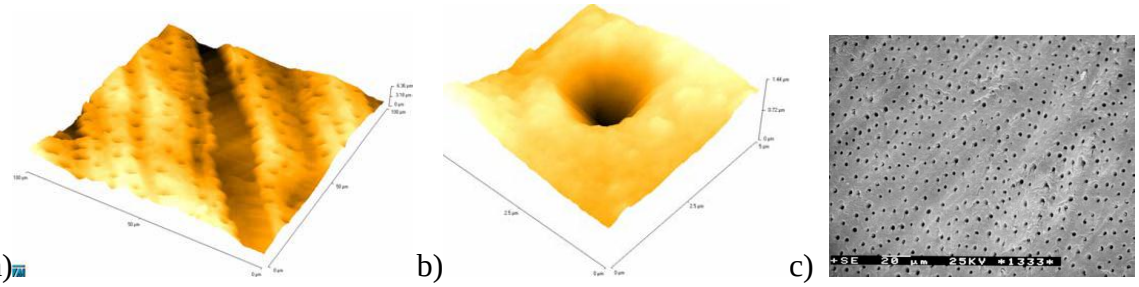

Figure 16. (a) Visible drafts on a surface of a dentin sample caused by mechanical preparation and depicted by AFM (scan range 100x100 µm) (b) 3D-image of dentin surface taken by AFM (scan range 5x5 µm) (c) The flat dentin surface with open dentinal tubules as seen by SEM (bar represents 20 µm) [42].

The authors point out that AFM brings new possibilities in imaging dentin surfaces since it is a non-destructive method [42]. More importantly, its main advantage is the capability to study samples under moist conditions, without having to chemically modify them. However; as every method does, it also has disadvantages such as being time consuming under some conditions. Authors also indicate that gathering meaningful statistical data from such a small area of the surface is very difficult.

Choi et al. [43] studied the effect of fluoride application on an enamel surface which was etched for 20s with 37% phosphoric acid. Images immediately after were acquired by

AFM and SEM (Figure 17). Noncontact mode AFM images were obtained using NANOstation II equipped with a 92.5 x 92.5 x 6 μm^3 XYZ scanner.

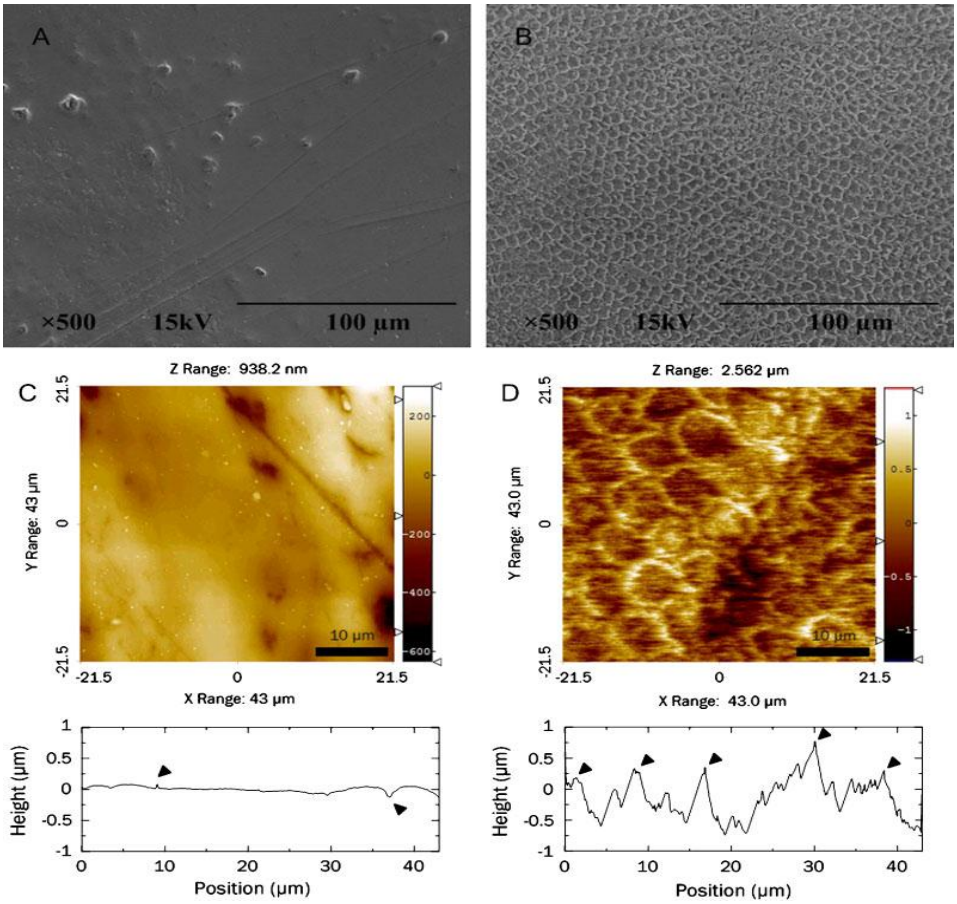

Figure 17. Representative SEM and AFM topographical images of permanent tooth enamel surfaces before (A, C) and after (B,D) acid etching for 20 s with 37 % phosphoric acid. The bottom panels show the line profiles selected randomly from those before and after etching [43].

The vestibular enamel surfaces of each tooth sample were scanned in air at a resolution of 512 x 512 pixels and a scan speed of 0.8line/s. Before etching images only show scratches and debris on the surface, while after etching images revealed enamel rod characteristics as well as showing that acid etching is effective in removing scratches and

debris from the surface [43]. Experiments were conducted with primary and permanent teeth which produced results to compare the two types of teeth in terms of acid resistance, acid etching patterns and enamel morphology.

1.7 Atomic Force Microscopy (AFM)

The atomic force microscope (AFM) was invented in 1986 by Binnig, Quate and Gerber, the same year in which Binnig and Rohrer won the Nobel Prize for Physics for developing the scanning tunneling microscope (STM). Binnig, Quate and Gerber essentially combined the principles of the STM and the stylus profilometer to create a characterization tool that incorporates a probe that does not damage the sample, works on both conductors and insulators, and can measure interatomic, electromagnetic and/or mechanical forces [44].

The Atomic Force Microscope (AFM) gathers data based on forces between a sharp probe and a scanned sample surface. The lateral resolution of resulting images depends on the tip geometry radius of curvature, which typically ranges between 10 and 50 nm. The resolution in the Z-direction is sub-nanometer.

The AFM probe itself is typically a cantilever with a very sharp tip at one end. While this probe scans the sample surface, a near-infrared laser beam is reflected off of the cantilever into a split photodiode. As the probe encounters attractive or repulsive forces during scanning, the cantilever necessarily reacts differently and hence the photodiode signal, changes. This signal is sent to a feedback-loop designed to maintain a constant

'setpoint' interaction by precisely driving the probe toward or away from the surface to return to the setpoint signal.

The AFM can be operated in a number of modes, depending on the sample and application. There are two main modes of imaging: contact mode, and AC mode (commonly known as 'tapping mode'[TM]).

1.7.1 Contact Mode AFM

In this operating mode, the cantilever deflection is used as a feedback signal and it actually represents the force applied to the sample surface. This force between the tip and the sample is kept constant during scanning by trying to maintain a constant deflection. The actual amount of force applied is highly dependent on the stiffness of the cantilever used. Therefore picking the right probe for each sample is crucial since there is a risk of damaging the sample as well as the probe itself.

1.7.2 AC Mode AFM

In this operating mode, the probe is in intermittent contact with the sample surface, with two benefits. First, lateral forces are minimized, diminishing friction and the chance of dragging or pushing features along the surface. In addition, the force gradient sensitivity allows lower maximum normal loads to be applied, minimizing tip/sample damage. The main principle is to drive the cantilever at or near its resonance frequency where the signal to noise ratio is optimized. Changes in the amplitude of cantilever oscillation are then used as the feedback signal instead of the lever deflection (though this can also be monitored). As the probe encounters differences in surface topography, the oscillation amplitude shifts. This shift triggers the feedback-loop, which tries to maintain the original

cantilever oscillation ‘setpoint’ by again by activating Z-axis piezoactuators to return to a preset tip-sample interaction. For imaging soft samples such as polymers and polymeric solutions, the AC mode is strongly preferred, and thus all AFM images presented in this report were gathered in AC Mode.

The typical initial set point for AC-mode using the Asylum Research mfp-3d hardware available in the nmLabs is 800mV, however this value often must be decreased to 10-50% of the starting (free) value for optimal image resolution.

Figure 18 shows a very basic representation of the major components of an AFM.

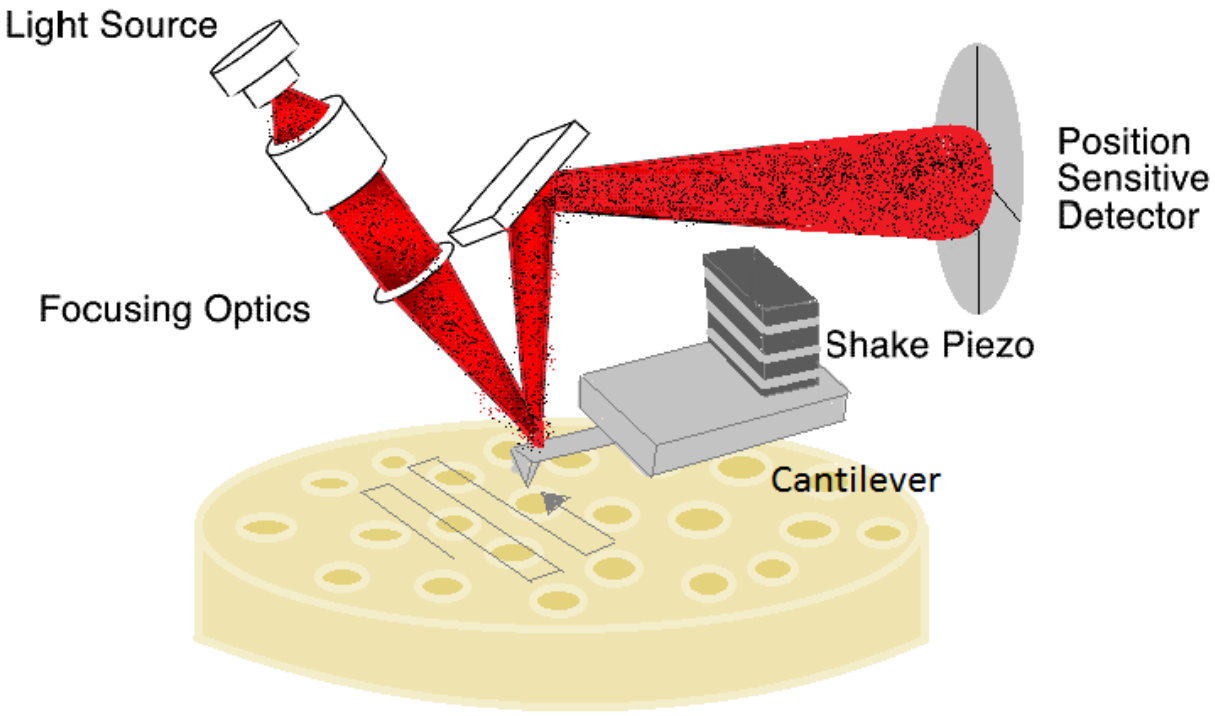

Figure 18. Schematic view of AFM head. Laser light is reflected off of the cantilever to the detector, signaling the piezo to move the probe up or down in order to maintain the pre-determined ‘setpoint’ force (laser spot on the detector) while scanning. The ‘shake’ piezo excites the resonant cantilever amplitude in AC mode imaging. (Image modified from[45])

Chapter 2: Materials and Procedures

2.1 Fuel Cell Electrode Sample Preparation

There are 7 different samples that are received from UTC. Three of the samples are so called “baseline samples” of initial materials, i.e. not manufactured fuel cell stacks. These samples include raw anode catalyst, anode floc, and Pt/C + phosphoric acid. The remaining four samples were tested / untested anode and tested / untested cathode assemblies, which are actual layers from real PAFC stacks.

The Anode catalyst is 10 weight % Pt/Vulcanized Carbon. The ***Anode floc*** comprises the anode catalyst described above, mixed with 46 weight % Teflon dispersion. The sample was mixed with a surfactant and blended under high shear. The Teflon dispersion is primarily ~200nm particles, with SEM indicating mostly single and double particles as well as 10-20% triplets. The ***Pt/C + phosphoric acid*** specimen was prepared by mixing 1.1507 grams of anode catalyst with 0.586 grams of 85% Phosphoric acid and enough water to make a paste. The paste was mixed by folding then put into TEFLON evaporating dish and heated in air overnight at 96 ˚C.

The **Anode catalyst** was in a fine powder form, which is very difficult to mount for AFM imaging. A piece of double sided tape was placed on a glass slide to collect powder sprinkled manually on top. After this process, distilled water was used to rinse the sample in order to rid the surface of loose particles which would otherwise interfere with AFM imaging.

Anode floc and **Pt/C + phosphoric acid** samples were in the form of dried crumbles of particles, sized on the order of millimeters and hence relatively easy to handle and mount.

Again for these samples, glass slides are used as a base on top of which a crumble was affixed with tape or superglue.

Tested/untested anode and cathode samples were also easy to handle and mount. For MFP 3D AFM imaging, the catalyst layer was cut into small pieces by a razor blade and peeled off of the carbon paper. They were handled with tweezers and fixed on glass slides with superglue at each corner. For Cypher measurements the mounting procedure is the same, except magnetic discs are used instead of glass slides.

2.2 Tooth Substrate Preparation

By the aid of a water-cooled, diamond bladed saw, horizontal, 800 um thick slices of dentin were cut from the crown section of human molars, slightly below the enamel-dentin junction. Typically, it is possible to obtain 2-5 usable specimens from each molar. The dentin slices were then polished on one side using 600 grit wet paper on a polishing wheel to create a uniform surface. The specimens were then further polished by using a polishing cloth (Microcloth®, Buehler, Lake Bluff, IL, USA), which was wetted with a 5 um alumina slurry.

Each specimen was polished until shiny, approximately 30 seconds. The specimens were then placed under a light microscope to confirm that a uniform surface was obtained. The shiny, polished side of the specimen behaves like a magnifier on printed text. The polished dentin slices were then placed in a jar of deionized water and sonicated for 10 minutes to remove the polishing abrasive. After sonication the specimens were rinsed with water.

Then specimens were etched in a Petri dish with a 1% citric acid solution in order to open the tubules. 20 seconds of mild back and forth agitation was used. After acid-etching, the dentin slices were rinsed with deionized water and then sonicated again for 10 minutes in deionized water. Finally, the etched and sonicated dentin slices were stored in a phosphate buffer saline solution (PBS, pH = 7). [37]

2.3 Polymer Solution Preparation

The polymer solution used in dentin deposition studies was applied as received throughout the range of experiments described. Several procedures for deposition were employed, including small volume drops from a 10 mL syringe, as well as larger drops followed by spin-coating. Details are provided in the appropriate sections which follow.

2.4 Conditioning and Coating Procedures

2.4.1 Active Solution on Graphite Substrate Imaged in Air

A fresh surface of the atomically flat graphite substrate was exposed by peeling the top most layers with double sided tape. The substrate was then coated with Active Solution. The solution was dropped on the substrate with a pipette and the sample was left to dry overnight. AFM imaging could be performed after 3 days of drying, although the sample visually appeared like it was not completely dry.

2.4.2 Untreated Dentin Substrate Imaged in Air

Untreated tooth substrates were preconditioned with deionized (DI) water for 10 minutes, and then immediately imaged in air.

2.4.3 2 min, 10 min and 1hr Treated Dentin Substrate Imaged in Air

Polymer solution was dropped on tooth substrates with a pipette until the entire surface was covered (usually 9-10 drops with a 10 mL syringe). These were then allowed to rest for 2 minutes, 10 minutes or 1 hour before rinsing with DI water. The rinse was performed by dipping the substrate once into a container filled with DI water. The samples were finally imaged in air after resting overnight in air.

2.4.4 1, 2, 3 and 10 Times Spin-Coated Dentin Substrate Imaged In Air

Polymer solution was dropped on the sample surface until the whole surface was covered. Next, a Laurel Technologies Corporation Model WS-400B-6NPP/ LITE spin-coater was used to distribute a thinner and more even layer. Each layer was spun with a speed of 3000 rpm for 30 seconds. Samples were imaged in air after resting in air overnight. Samples were not preconditioned before spin-coating.

2.4.5 Brushed and Spin-Coated vs Spin-Coated Only Dentin Substrate Imaged in Air

Tooth samples were brushed for 15 seconds with commercial Toothpaste using a circular motion and a force of approximately 50 grams (measured by brushing while mounted on a scale). Next the samples were rinsed with DI water in a Petri dish using very mild fluid agitation with a magnetic stirrer. After rinsing, the samples rested in air for 2 minutes.

Finally, 20 spin-coats with Active Solution were deposited based on the same spinning parameters as described above. Related specimens, 'spin-coated only,' were prepared with the same procedure except they were not brushed.

2.4.6 1 month Old, Spin-Coated Only Dentin Substrate Imaged in Fluid

The spin-coated only sample mentioned above (not also brushed) was placed in an AFM fluid imaging chamber flooded with DI water, 1 month after its preparation following sitting in air. The sample was spin-coated 20 times with polymer solution after being preconditioned with DI water.

2.4.7 Spin-Coated Dentin Substrate Rested at 37°C, Imaged in Air

A dentin disc was coated 10 times with Active Solution by the spin coater. It was not preconditioned before coating. Then the sample was placed on a glass slide and warmed on a heater at 37°C - 40°C in air for 2 days.

2.4.8 Spin-Coated Dentin Substrate Imaged in Fluid with iDrive

A dentin disc was coated 10 times with Active Solution by the spin coater. It was preconditioned with DI water before coating. AFM imaging was done between successive spins.

2.5 AFM Imaging

Two different models of AFM were used throughout this study. An Asylum Research MFP-3D AFM with integrated inverted optics (Nikon TE-2000) was used for imaging dentin samples. The Asylum Research Cypher was used for imaging fuel cell electrodes. Both AFMs are operated with Igor Pro 6.22A with MFP3D 101010+1202 plug-in.

For AC mode imaging of dentin discs in air, Al reflex coated Si cantilevers (Model: AC240TS) were used. These 240 um long, rectangular cantilevers are manufactured by Olympus and have 2 N/m of spring constant, 70 kHz resonant frequency and Si tetrahedral tips with approximately 10nm radius. Some measurements in fluid were also performed with Olympus AC240TS probes based on standard acoustic (piezoactuated) vibrations.

"iDrive", a new hardware for liquid imaging, was used for the bulk of the fluid imaging of dentin samples. This equipment uses Lorentz Forces to electromagnetically actuate a specially microfabricated cantilever using an oscillating current flowing perpendicular to a nearby magnet. "iDrive" requires a special cantilever holder which is a modification of the normal piezo-actuated MFP3D holder to retains piezo-driving functionality, but can also be easily switched for electromagnetic actuation. Utilization of "iDrive" requires special cantilevers. The probes used in the dentin study were AR-iDrive-N01 BL-TR400PB. These are 100 um long, triangular shaped silicon nitride cantilevers with around 32 kHz of in air resonant frequency, which drops down to 10 kHz in fluid due to fluid damping effects.

For AC mode imaging of PAFC electrodes, the Asylum Research Cypher was employed. In order to be able to resolve nanometer scale particles and pores of these samples,

Nanosensors SuperSharpSilicon SSS-NCH-16 probes were used. Resonant frequencies of these 125 um cantilevers are typically between 260 and 410 kHz (mostly around 330 kHz), and their spring constants are roughly 42N/m. Their tip radii are less than 10 nm.

To set up the experiment for "in-air" AC mode imaging of dentin samples, first an Olympus AC240TS tip was mounted to the head of the AFM. The sample was mounted on a glass slide by using super glue. Through the Igor software, the overhead optics are used to locate the cantilever and align the laser beam. The laser is aligned in a way that maximizes the overall signal in both the x and y direction while keeping the beam as close as possible to the tip of the rectangular cantilever. The initial lever deflection is then fixed at zero. An auto-tune of the resonant frequency of the cantilever was finally performed so that the head of the AFM could be engaged to the sample surface with the constant-interaction-maintaining feedback loop enabled. A scan size as high as 40 um was used in order to visualize a large number of tubules since their normal diameters are approximately 4um. The scan size was decreased from 40um to 15um, 5um and finally 1um to be able to resolve all features in relevant length scales. Overhead optics was also utilized from time to time to identify new scan areas.

Piezoactuated AC imaging of dentin samples required several additional steps to what has already been mentioned. Since the shake piezo oscillates the entire cantilever holder, this generates standing and transient acoustic waves in the fluid chamber resulting in a 'forest of peaks' when sweeping the drive frequency, only some of which provide adequate imaging. Hence, finding the actual resonant peak of the cantilever becomes very difficult. To overcome this issue, after setting the deflection to zero (essentially contacting the tip on the sample), a 100 count thermal data was captured (spectrum of thermally excited

amplitude versus frequency). Appending this result with the forest of acoustically excited peaks allows one (or an experimentally testable handful of) amplitude peak(s) nearest the lever resonance to be identified and tested for image quality. Finally, the head was engaged on the sample mounted on a coverslip by using super glue. The coverslip was contained in the fluid chamber of AFM which was filled with 1mL of the fluid of interest.

"iDrive" imaging was performed following almost the same steps as for "in-air" AC imaging, though of course the special "iDrive" cantilever holder was mounted to the head of the AFM. Software directly recognizes this special holder and a "check" sign appears next to the "iDrive" option located in the "Tune" tab of the AFM software. After optimizing the sum signal and setting the deflection to zero, an auto tune of the resonant frequency can be easily performed since only one peak, instead of a forest of apparent resonances, is apparent. Otherwise, tip approach and imaging are as before. The sample was mounted the same way as for acoustic excitation as well.

In-air AC imaging of PAFC electrodes was performed by using the AR Cypher AFM. The samples were superglued on 15 mm diameter magnetic discs. A Nanosensors SuperSharpSilicon tip was mounted on the special holder for Cypher and the probe was brought within close proximity to the sample using the software controlled approach and focusing motors. When ready, the probe was brought to a safety height -with a one button click- where the tip-sample separation is 50 um. The lever resonance was auto tuned to its resonant frequency in air, and was engaged on the surface automatically for imaging.

Chapter 3: Fuel Cell Electrodes

3.1 Fuel Cell Electrode AFM Results

3.1.1 Anode Catalyst

Figure 19 shows height and phase images of the anode catalyst with blue and yellow color contrast, respectively. In these images the particle size appears to be less than 100 nm based on the smallest feature sizes resolved, which is expected of the carbon black and Pt particles. A strong phase contrast does not exist as anticipated, excepting edge effects which correlate with feature edges in the height data.

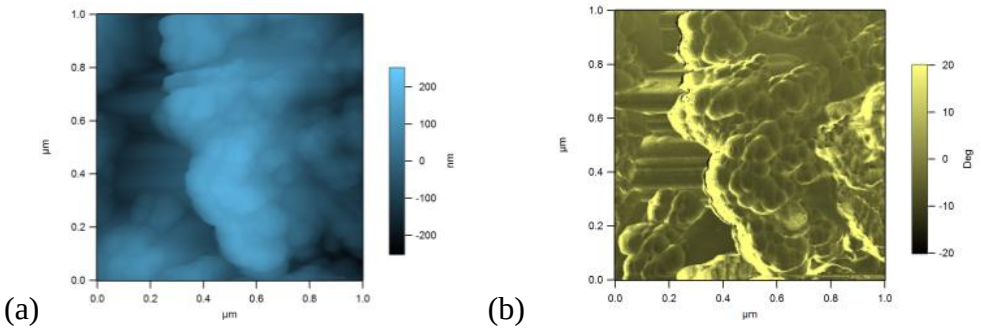

Figure 19. (a) 1 um AFM images of anode catalyst sample (a) Height, (b) Phase

3.1.2 Anode Floc

Figure 20 shows height (blue) and phase (yellow) images of the anode floc sample. This specimen includes the anode catalyst layer mixed with PTFE which has a bigger particle size. The images clearly show the particles or clusters have become larger than the initial (uncoated) 100nm features. Again, phase contrast is relatively weak, simply supporting the height data.

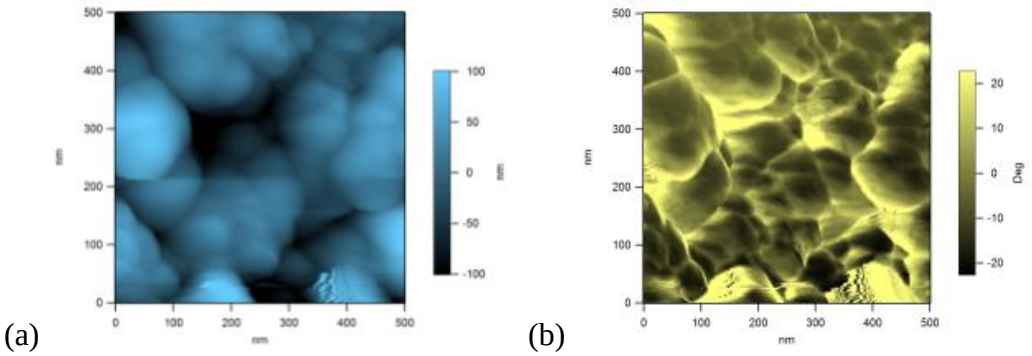

Figure 20. 500nm AFM images of anode floc sample (a) Height, (b) Phase

3.1.3 Untested Cathode

Figure 21 shows the untested cathode morphology which is expected to give similar results to the floc sample. Especially in the 500nm images, it is clear that the particle size is larger than 100nm. In the 1um height image, there seems to be some smaller particles which are less than 100nm in diameter as well. These could possibly be carbon black + Pt particles which were not evenly coated with PTFE.

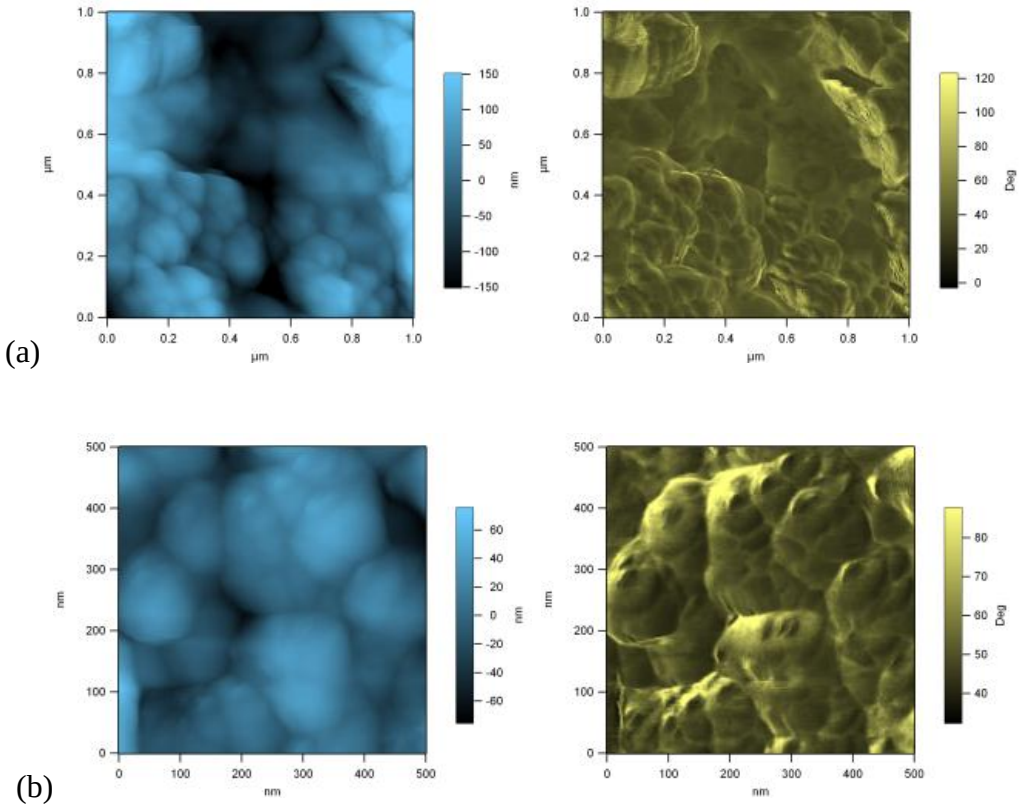

Figure 21. AFM images of untested cathode sample (a) 1 um Height (blue), 1um Phase (yellow), (b) 500nm Height (blue), 500nm Phase (yellow)

In another set of experiments, cathode images with different features were observed. Figure 22 shows these images which reveal fibrils of a material on the particles. These fibrils are very similar to the ones observed in the SEM images of Choi et al. [20] who investigated the shape and microstructural evolution with temperature of PTFE in the electrocatalyst layer made of various Pt-C composites. As a result, they concluded, these fibrils were not formed during the fabrication process but rather were present as a raw material component of the initial PTFE supply.

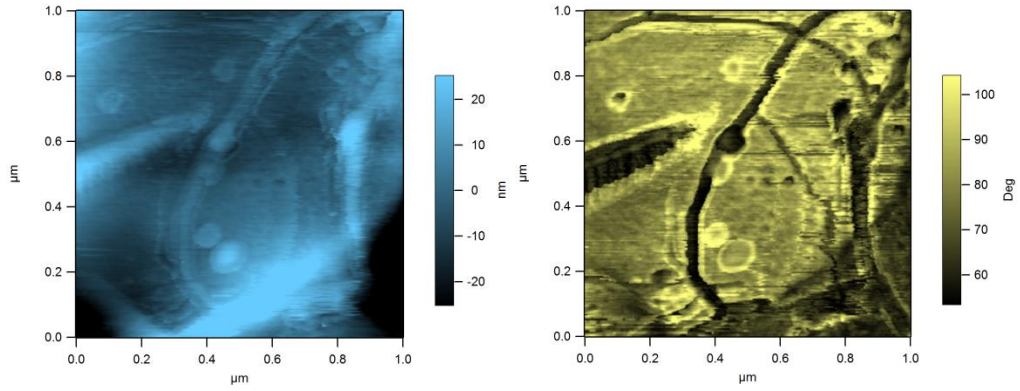

Figure 22. AFM images of untested cathode sample with PTFE fibrils - 1 um Height (blue), 1 um Phase (yellow)

3.1.4 Untested Anode

Figure 23 shows the untested anode morphology, which is expected to give similar results to the floc sample as well. In the 1um images in (a), a mixture of particle sizes is observed indicating an uneven PTFE coating on the surface. Linear streaks are apparent as well, particularly in the phase images, which are likely tip artifacts as the actual shape of the AFM probe interacts with various edges on this highly porous surface. In some manufacturing conditions, however, Teflon particles are known to elongate and form 'strings,' which is another possible explanation for the linear features.

In the (b) images the effect of PTFE coating is very clear again, making the particles bigger than 100nm.

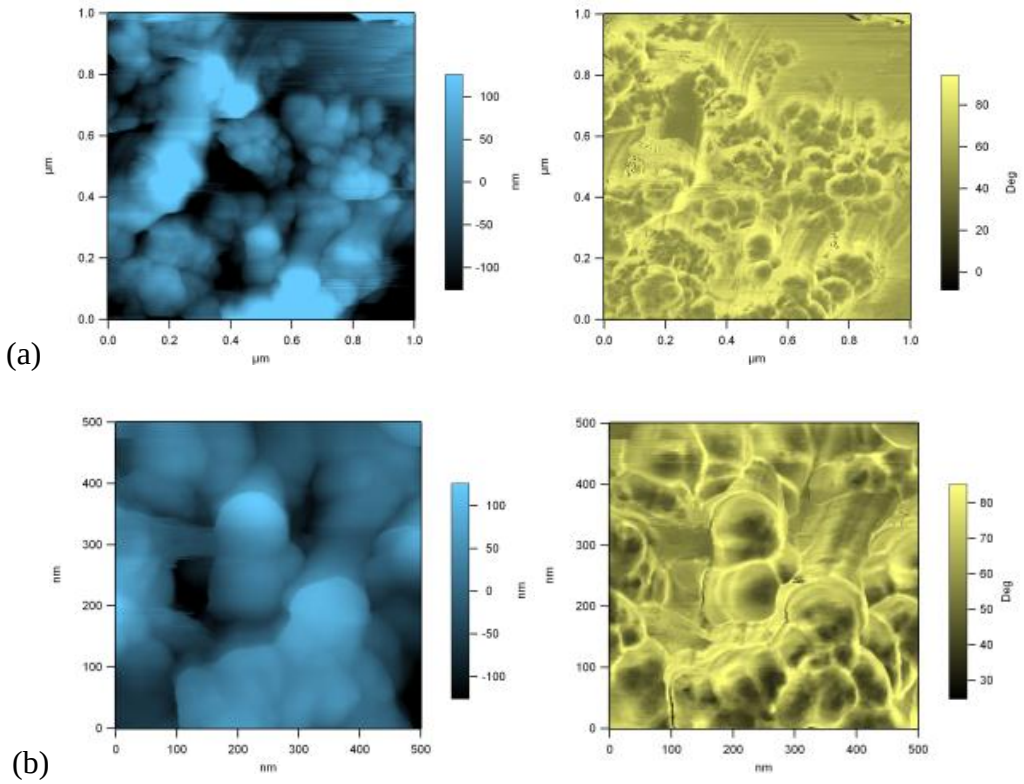

Figure 23. AFM images of untested anode sample (a) 1 um Height (blue), 1um Phase (yellow), (b) 500nm Height (blue), 500nm Phase (yellow)

3.1.5 Pt/C + Phosphoric Acid (PA)

Figure 24 shows the morphology of carbon black and Pt particles coated with PTFE and loaded with PA. In both of the height images there are various tip artifacts which make it difficult to observe the particle size; however PA loading clearly changed the morphology. Furthermore, phase images show a significant increase in contrast (at least 2X) in comparison to unloaded specimens. Some heterogeneity in PA loading from location to location is also observed, though not as substantial as anticipated based on separate data.

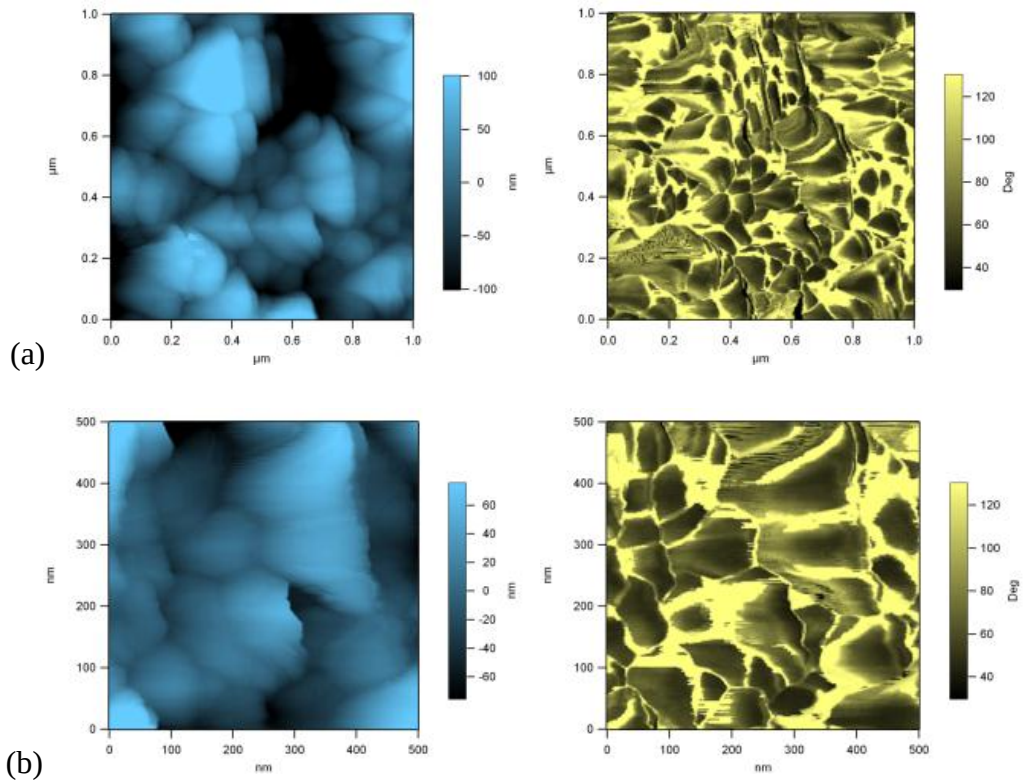

Figure 24. AFM images of Pt/C+PA sample (a) 1 um Height (blue), 1um Phase (yellow), (b) 500nm Height (blue), 500nm Phase (yellow)

3.1.6 Tested Cathode (PA impregnated)

Figure 25 shows topography and phase images of the PA loaded cathode sample. In this case, the images clearly reveal material removed from some particles following PA loading. This is most likely PTFE coating separating from the underlying catalyst particles. Phase contrast is remarkably strong in these locations, with magnitude consistent with particle/PA contrast but morphology possibly suggesting particle/PTFE contrast. The thickness of the removed material is measured to be 3.2 nm with ±1.3 nm standard deviation based on topography image cross-sections. The necessary intimate

contact between these distinct layers therefore can be lost, which would substantially degrade fuel cell performance.

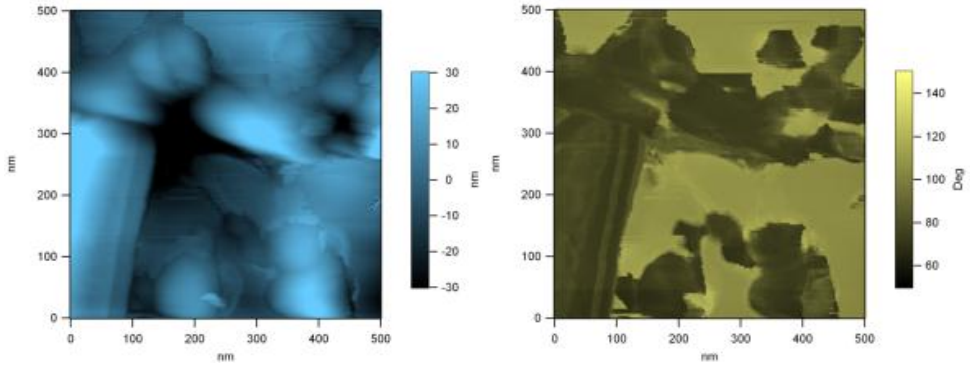

Figure 25. AFM images of tested cathode sample - 500nm Height (blue), 500nm Phase (yellow)

3.1.7 Tested Anode (PA impregnated)

Figure 26 shows similar measurements but for the tested anode. While linear streaks are again apparent suggesting either porosity-induced image artifacts or Teflon elongation during manufacturing, no evidence of layer separation occurs as with the tested cathode.

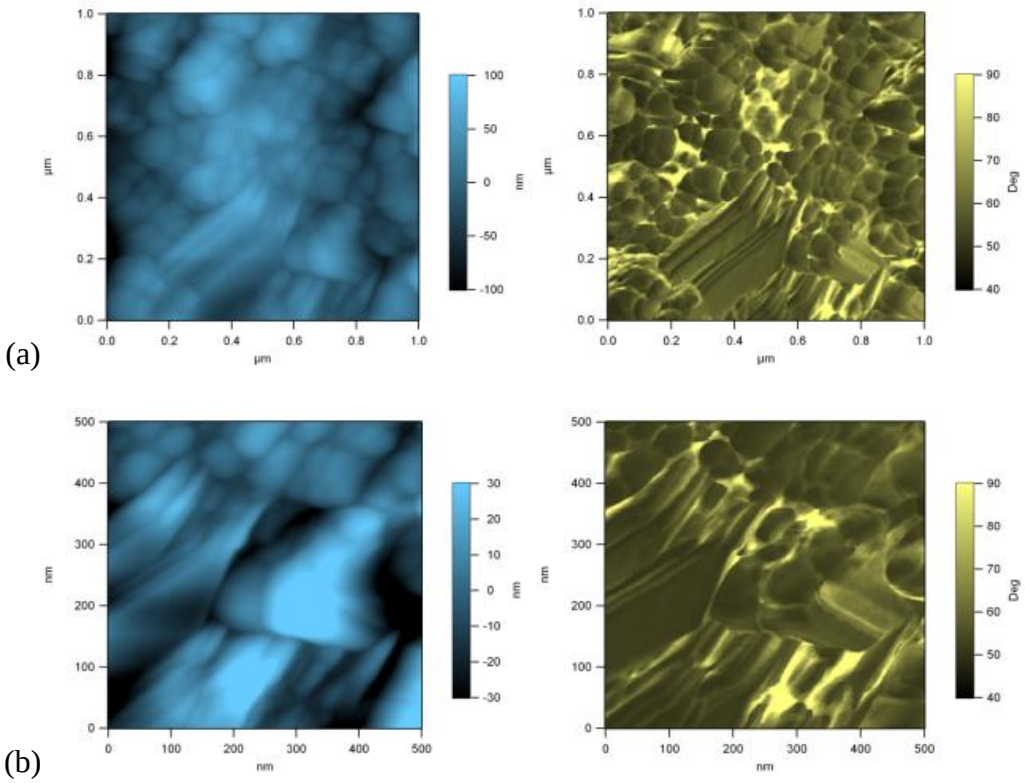

Figure 26. AFM images of tested anode sample (a) 1 um Height (blue), 1um Phase (yellow), (b) 500nm Height (blue), 500nm Phase (yellow)

3.2 Experimental Challenges

It is always difficult to image highly porous samples with AFM. The PAFC electrodes are such materials with highly varying particle and pore sizes providing optimal transport properties for gas and liquid phase diffusion, but completely at odds with optimal AFM imaging conditions. To be able to resolve all the features on the surface, custom

sharpened AFM probes were employed, which unfortunately are prone to fracture at the apex (becoming blunt) and relatively expensive to start with. Necessary scanning conditions for such fragile tips are slower scan rates (which increase the total scanning time) on the order of 2 to 5 seconds per line, and higher feedback gain values of approximately 20 (which can increase background noise, compromising the image quality).

Another challenge encountered was long distance forces between the sample and the tip, which caused the AFM system to falsely 'engage' on the surface even though the tip was still significantly far away from the sample. To overcome this issue, the resonant frequency was successively re-tuned and the surface approached further each time the AFM thought the surface was present, until a stable signal and stable imaging was feasible.

A frequently encountered problem especially with imaging the catalyst materials involved particles and/or clusters becoming attached to the tip, creating image artifacts. When this occurs, the frequency of the cantilever shifts abruptly since mass is added to the vibrating resonant system. This dramatic change in frequency can be clearly observed by performing a new resonant frequency auto-tune. In these cases, drive frequency and drive amplitude of the cantilever were maximized in order to dislodge any contamination on the tip, or the tip was disposed of and a brand new probe was utilized instead.

3.3 Future Work

For PAFC electrode catalyst layers, future work should ideally focus on targeted specimens which are expected to exhibit morphology variations in the particle, coating, and/or impregnation morphology based on preliminary SEM or performance evidence supplied by the project collaborators, in order to thoroughly understand the microscale and nanoscale structure of the various components. In-situ measurements of current conduction and especially heterogeneities in a working or cycled fuel cell would also be interesting academically and industrially.

Chapter 4: Dentin

4.1 Model Systems

Prior to imaging dentin structures and their morphology upon exposure to polymeric films, several model systems were investigated. These include graphite as an ideally flat substrate, and alumina nanoporous membranes as a system with optimally small pores, as described below.

4.1.1 Polymer on Graphite Substrate Imaged in Air

AFM images of the polymer solution on an atomically smooth surface, graphite, were first acquired in order to understand the behavior of the polymer without the interference of substrate morphology. The lighter colored patches (protruding) reveal nanoscale islands of the polymer wetting the substrate in a representative topography image,

Figure **27** (left). Phase contrast (right) compliments the topography data indicating a distinctly different tip-surface interaction betweenn the Si probe and the graphite (bright) or polymer islands (dark). The AC-AFM amplitude image (center) merely highlights feature edges.

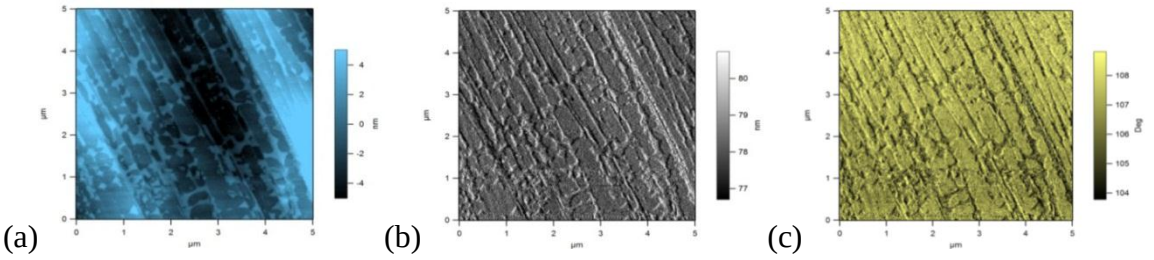

Figure 27. AFM images of polymer solution on atomically flat graphite substrate, (a) Height, (b) Amplitude, (c) Phase

Clearly the polymer solution did not cover the substrate perfectly. Better wetting could undoubtedly be achieved by engineering the surface energy at the substrate through self assembled monolayers, selection of different substrates, etc. Since the aim of this project relates to teeth, however, this model system was simply intended to test whether imaging of the relatively tacky polymer is possible at all once deposited onto a substrate.

Taking this concept a step further, Figure 28 shows six successive topography images taken at the same location. A 256 x 256 image requires 4.3 minutes to be recorded at 1 Hz. According to this, if Image 1 was taken at time = 0, Image 6 was being taken almost 20 minutes after. There is a clear morphology change as the scanning continues on one spot which is $5um^2$ in size. It appears that the polymer islands spread as a function of time, for which there are a few possible explanations. This could be due to the presence of a larger reservoir of polymer out of the field of view, which continuously flows into the imaged region during the span of the experiment. Optically there is no evidence of such a reservoir, though it is nevertheless possible given the thin nature of the film and the optical resolution of the microscope as configured.

The tip may also be redistributing the material over the imaged area during scanning. This may be due to simple lateral forces, or alternatively the rapid normal motion of the AFM probe during AC-imaging may be locally heating and/or melting the polymer, encouraging flow. For this measurement, an Olympus AC240TS tip was used in air, with a resonant frequency of approximately 70 kHz. At a scan rate of 1 Hz on a 256 x 256 image, the tip spends 2 msec per pixel. This equates to the tip touching each pixel 140 times, in an effective area of 19.5nm x 19.5nm = 380.25 nm^2. Similar observations,

including damage and even melting, have been initiated in this manner on other polymer systems.

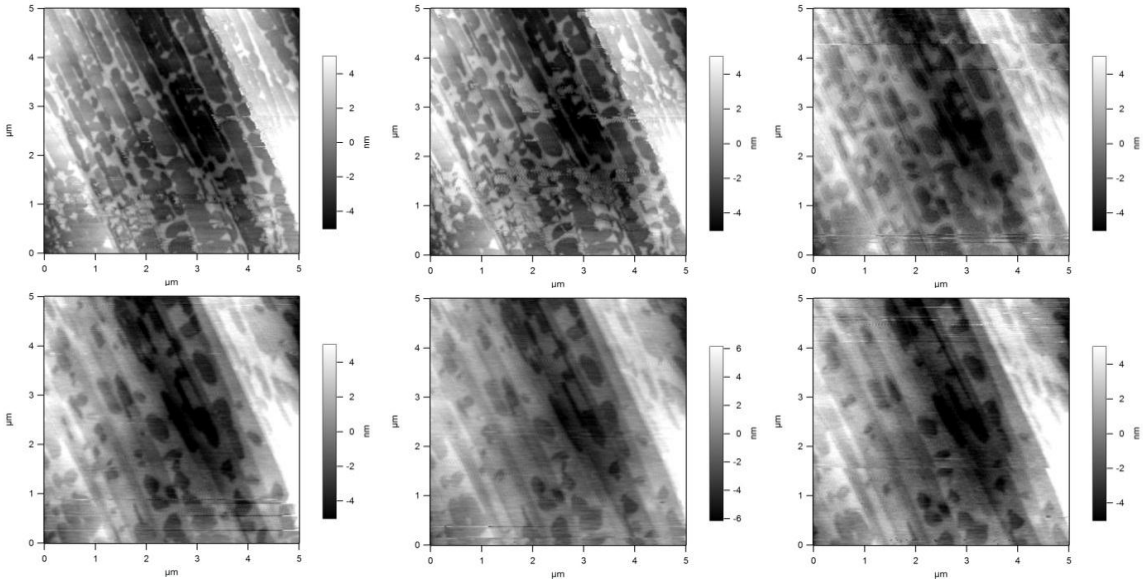

Figure 28. Successive topography images of polymer solution on graphite showing spreading islands as a function of time

Most probably, the features are islands which initially formed driven by surface energy incompatibilities between the polymer and the substrate. These may simply be spreading with time during the image sequence in Figure 28, presumably mediated by humidity from the ambient conditions during the AFM imaging. This is the most plausible explanation, since the feature height in fact decreases over time as shown in Figure 29. The same five features were analyzed on each successive frame by taking cross sections on the feature and determining the step height (dZ) between the light colored and dark colored regions. This enables the height of the polymer deposition (light) with respect to the underlying substrate (dark) to be accurately monitored. Such results indicate that the polymer is capable of coating a smooth surface, spreading to coat it, and that this process

can be imaged with AFM. The remainder of this chapter focuses on polymer interactions with more realistic porous structures.

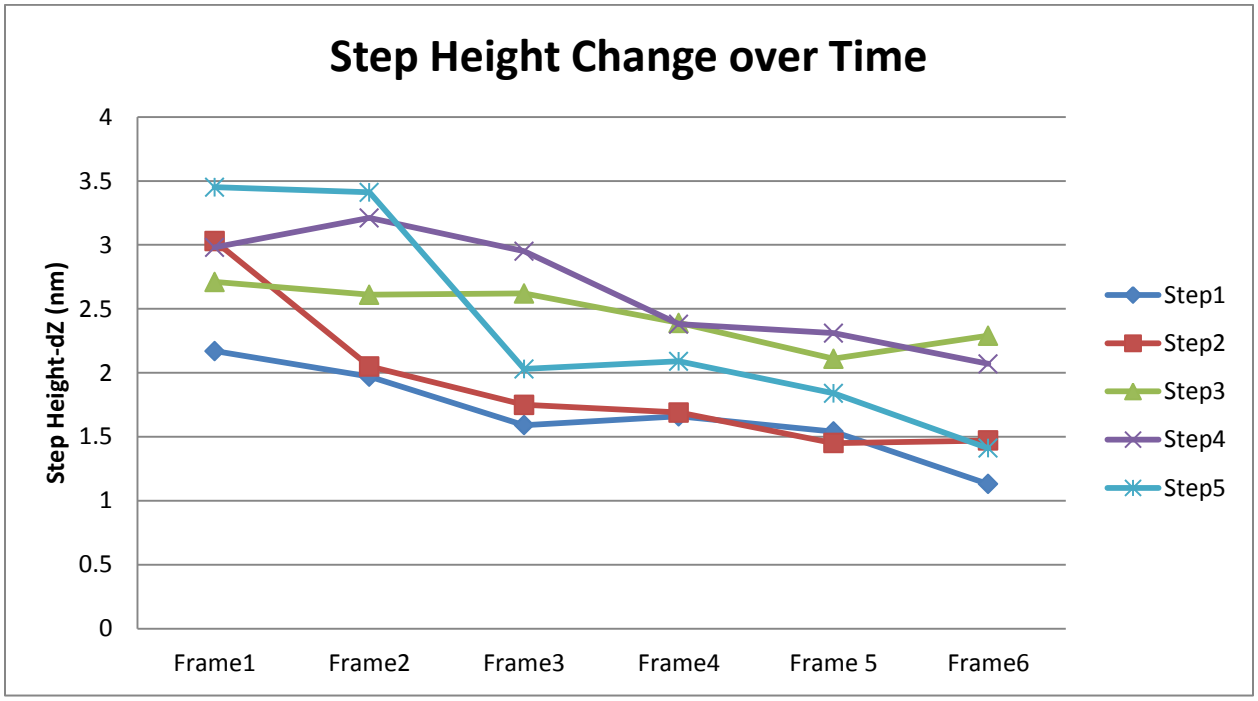

Figure 29. Plot of the decrease in feature height over 6 successive images

4.1.2 Polymer on Alumina Nanoporous Membranes

In order to consider the effect of polymer deposition on a substrate with fine pores, a Whatman Anodisc Alumina Membrane of pore size 200nm was covered with the solution by spin-coating. This membrane sample has a 25mm diameter. AFM imaging was performed on bare samples, as well as those spin coated with polymer 3 times, 6 times, 9 times and 12 times. The images Figure 30 and Figure 31 are 5um AFM height (blue) and phase (yellow) images.

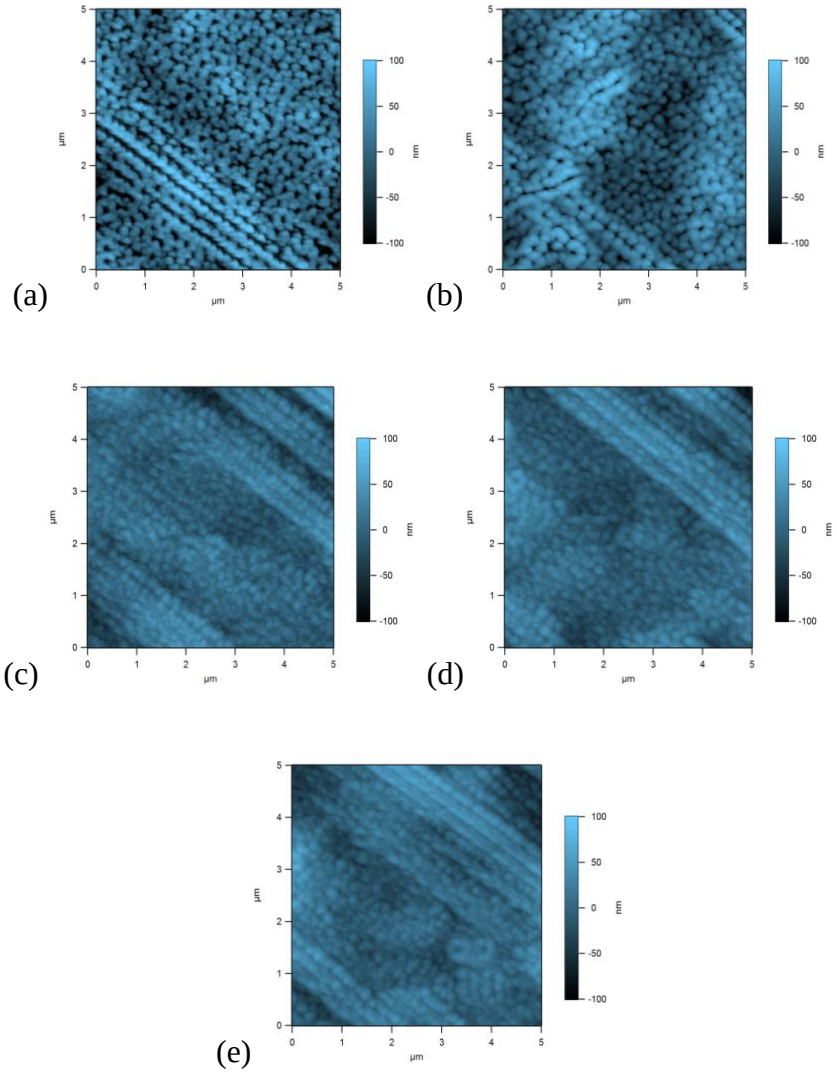

Figure 30. Successive topography images of Whatman Anodisc Alumina Membrane (a) Bare, (b) 3 times coated, (c) 6 times coated, (d) 9 times coated, (e) 12 times coated.

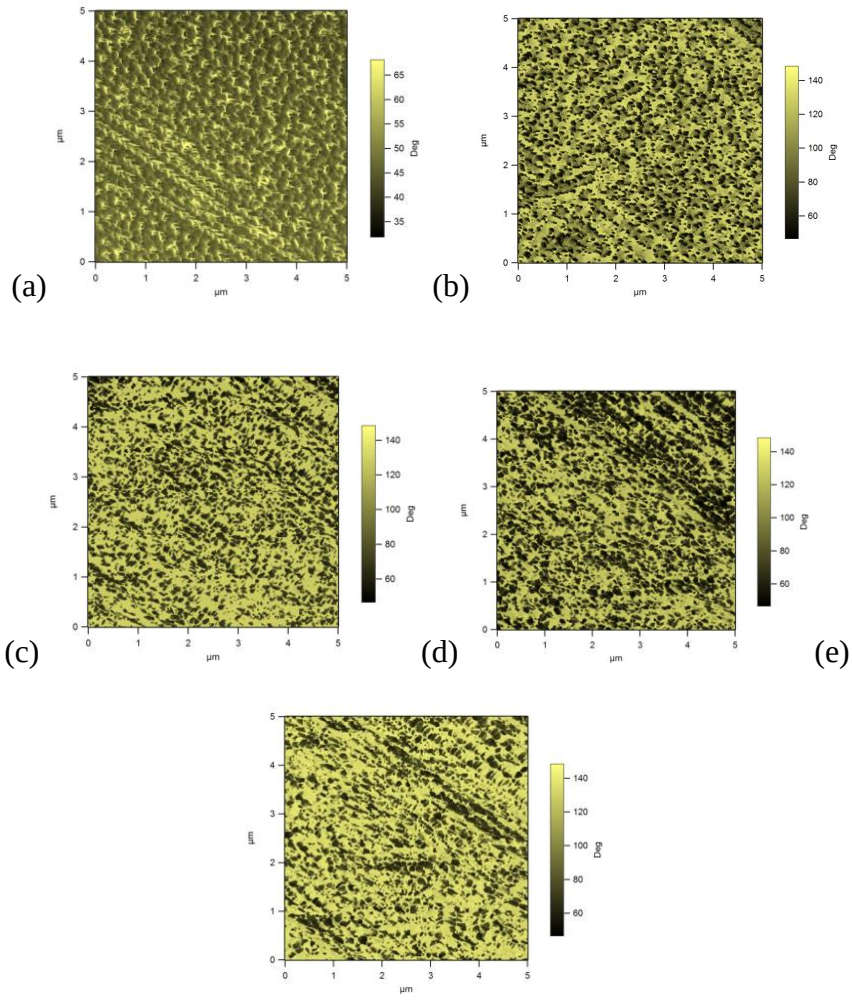

Figure 31. Successive phase images of Whatman Anodisc Alumina Membrane (a) Bare, (b) 3 times coated, (c) 6 times coated, (d) 9 times coated, (e) 12 times coated.

The successive height images (in alphabetic order) can be seen to generally become smoother as the number of spin-coating layers increases, suggesting a gradual coating of the exposed surface and possibly the pores as well. Phase images support this observation, with the relative fraction of one surface component (bright contrast corresponding to the polymer) increasing from left to right. Eventually, the polymer spans many of the pores, obscuring an ever-increasing fraction when comparing the early and final stage images (different, but representative, surface locations).

4.2 Dentin Results

This section deals with imaging teeth without and with, exposure to the polymer.

4.2.1 Untreated Dentin Substrate Imaged in Air

AFM imaging on bare dentin surfaces was first carried out in order to visualize the initial morphology before polymer exposure. Dentinal tubules averaging 4 um in diameter, and much smaller collagen fibers oriented randomly within the dentin, are visible due to demineralization of the dentin by acid, following the standard specimen preparation procedures (without etching, a ‘smear layer’ obscures most tubules). These samples are from molars of different humans, cross sectioned at varying tooth locations, and hence features sizes, periodicities, and relative ratios of collagen within the dentin vary from sample to sample. The images of Figure 32 are representative of these varied structures, at length scales spanning 40 um down to 1 um on a side.

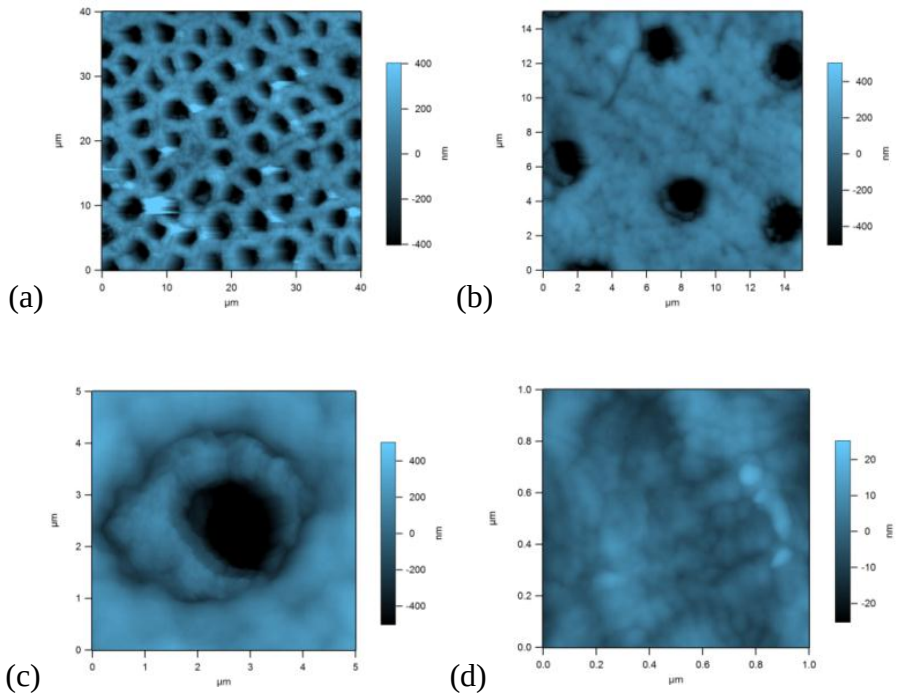

Figure 32. Untreated dentin substrate topography images at length scales (a) 40um, (b) 15um, (c) 5um and (d) 1um

The bare teeth were imaged in air after pre-conditioning in deionized water. Tubules can be observed in the first three images since the image size permits. In the rightmost image which shows a 1um^2 area, collagen morphology can be observed. The repeating units are in the order of 60-70 nm which is in agreement with the literature.

4.2.2 2 min, 10 min and 1hr Treated Dentin Substrate Imaged in Air

Teeth were next exposed to the polymer for varying durations from 2 minutes to 1 hour. Specifically, a drop of polymer was left on the tooth substrate for the noted time before rinsing and then AFM imaging in air. The resulting AFM height images are shown in Figure 33. Unlike in Figure 30, the polymer did not appear to span the tubules with the exception of the much larger clusters apparent only after 60 minutes of deposition. There is the possibility that these large clusters are in fact dust captured by the tacky polymer

during the extended air drying period, though this is unlikely given their dimensions: approximately 5 um disks, but only 400 nm thick (particles from the environment are typically more symmetric).

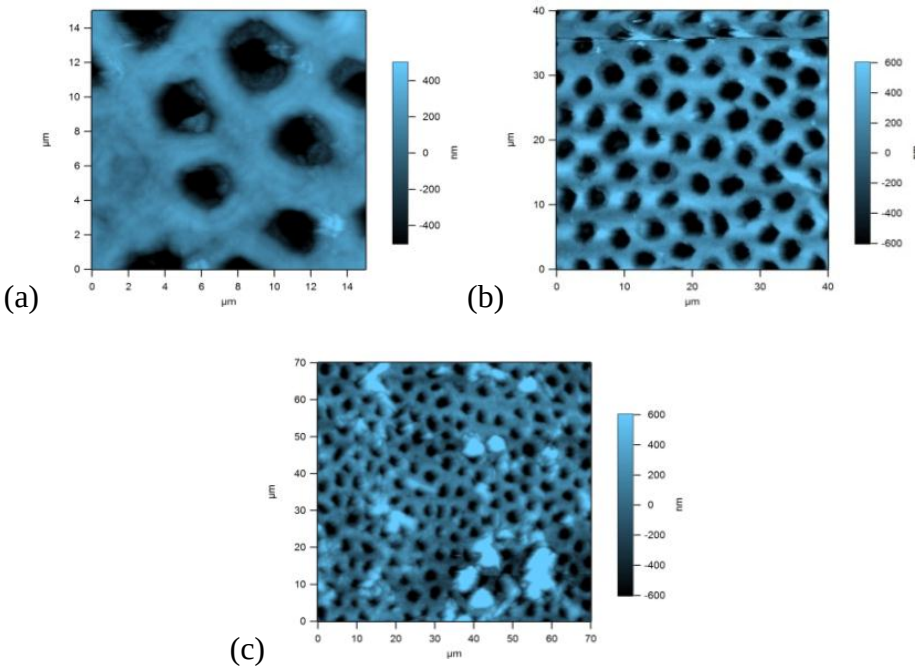

Figure 33. Topography images of dentin substrate exposed to polymer solution for (a) 2 minutes, (b) 10 minutes, (c) 60 minutes.

4.2.3 1, 2, 3 and 10 Times Spin-Coated Dentin Substrate Imaged In Air

Simple polymer drop casting as considered above generates uncertainty in the polymer thickness, and therefore the experiments primarily shifted to deposition via spin coating to deposit a much more uniform volume from one specimen to another. This furthermore can achieve a more homogeneous layer, as well as a thinner layer in order to facilitate imaging in a shorter period of time following deposition (faster drying). The development of the polymer coating morphology from one successive spin coating layer to the next

was imaged as in Figure 31. Again, though, the imaged areas were not identical from one layer to the next due to substantial challenges in finding the same location once the surface is obscured optically and topographically by the polymer deposition (hiding any underlying marks useful for registration of separate images).

40 um, 15 um and 1um height images (top to bottom) for increasing coating counts (left to right) are shown in Figure 34. It is very clear that as the number of layers increases, the nanostructured surface features become less apparent. This is especially obvious upon comparison of the 1 um images (bottom row). The leftmost frame (1 layer) clearly reveals a rope-like collagen fiber extrusion. Nano scale island patches are also apparent, as with the polymer deposited onto graphite,

Figure **27** (a) and Figure 28. The second image (2 layers) shows a mixture of dentin/collagen and smooth polymer regions, while the third frame (rightmost, 3 layers) shows a completely smooth morphology.

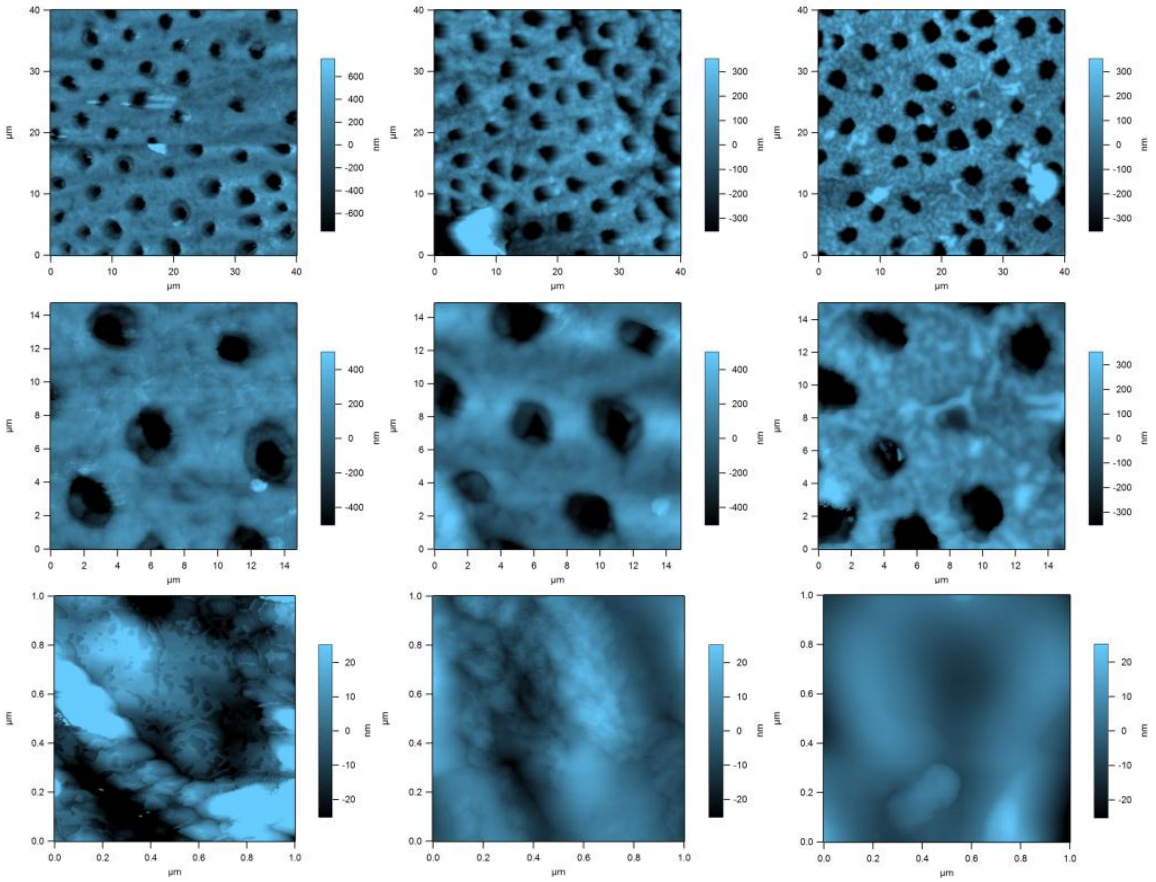

Figure 34. 40 um, 15 um and 1um topography images (top to bottom) for increasing coating counts; 1layer, 2layers, 3 layers (left to right)

In addition to the dentin/collagen being coated by the polymer after the 3rd spin coating layer, the polymer is also observed to have partially spanned one of the tubules (center row, right column). The structure just to the right of the center of this 15 um image is halfway obscured. This may be indicative of a necessary number of polymer depositions to span the large pore areas, or could related more to a necessary binding time for the polymer to sufficiently attach to the dentin/collagen, and itself, that it does not detach during rinsing.

It is interesting to consider the influence of polymer coatings on the tubules themselves, whereas much of the previous work emphasized the coating on the dentin and/or collagen. In Figure 35 and Figure 36, 15 um and 5 um height images and cross sections are shown. When images with larger scan sizes are compared, (a) and (b), obviously there is a substantial difference between the depths of tubules as revealed by the cross sectional data. These samples are each spin-coated with 10 layers, though one is masked, inhibiting polymer attachment and/or infiltration into the tubule. In the cross section image of (a) the depth difference between surface and trough (cursor points in the figure) is 158 nm, whereas in (b) this difference is 1.35 um.

(a)

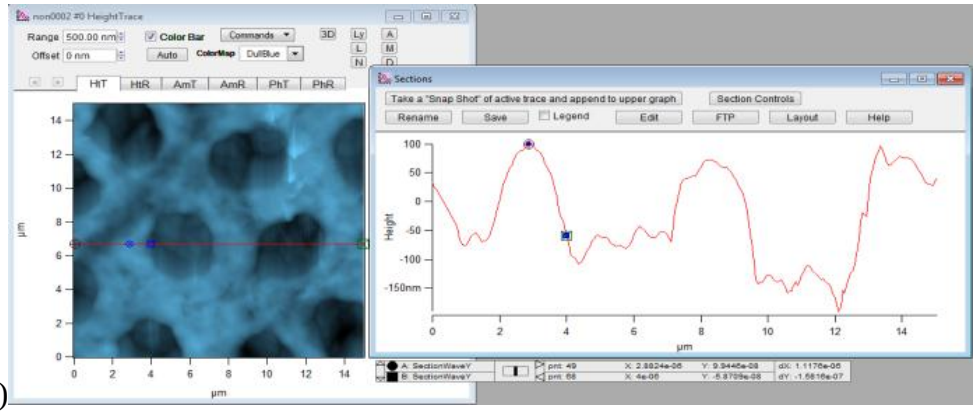

(b)

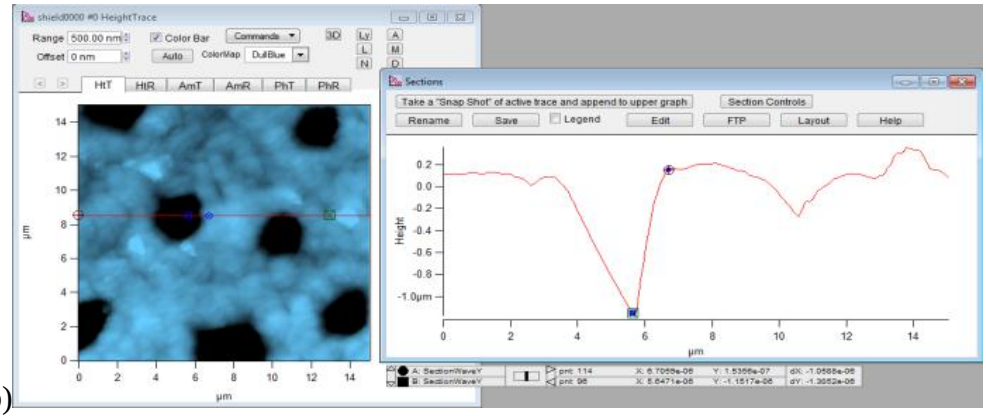

Figure 35. 15 um Height image and cross section of (a) 10 times (b) 3 times spin coated tooth

A zoomed in height image and the associated cross section plot are also shown in Figure 36, (a) and (b) respectively. These two reveal a similar difference in polymer occlusion of the tubules.

(a)

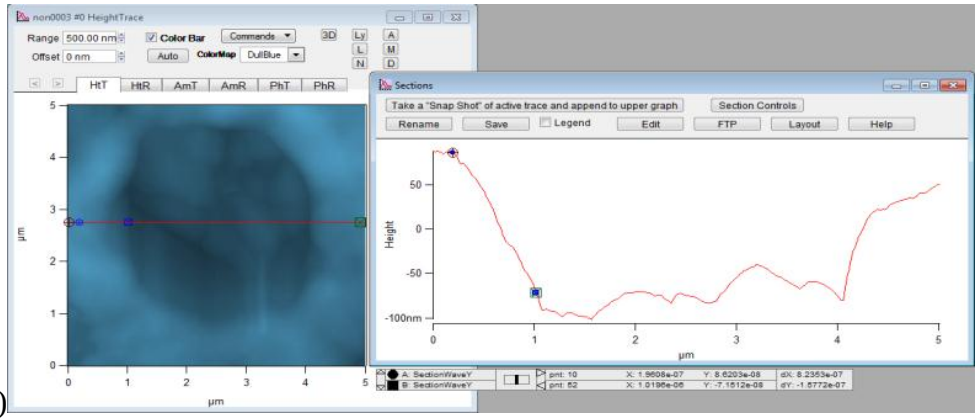

(b)

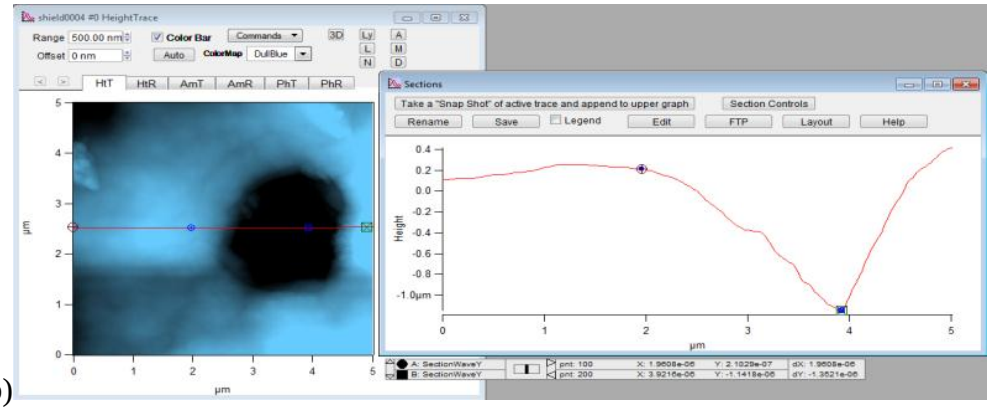

Figure 36. 5 um Height image and cross section of (a) 10 times (b) 3 times spin coated tooth

4.2.4 Brushed and Spin-Coated vs Spin-Coated Only Dentin Substrate Imaged in Air

To more precisely relate to in vivo conditions, images of polymer coatings on teeth that were brushed with commercial toothpaste before deposition were compared with polymer coatings for teeth that were not brushed (as above). In Figure 37, 15 um (left) and 5 um (right) topography images of coated (1st row) versus brushed and coated samples (rows 2 and 3) are shown. For the brushed and then polymer coated samples, particles present in the toothpaste clearly decorate the dentin surface (middle), possibly interacting with the following polymer deposition. The surface morphology of the specimen changes drastically with the incorporation of these toothpaste particles (100-500 nm), which are significantly smaller in size than the diameter of the tubules (4 um). In some cases (base), the toothpaste particles and/or polymer are even seen to cover the whole surface, even going inside the tubules and decreasing their apparent diameter significantly. The polymer may play an important role in binding the particles; a comparative study of brushing and particle assembly alone could not be performed. Note that the quality of the higher resolution images appears worse, though this is primarily an artifact related to the particle size approaching the size of the AFM tip, the relative pixel size, and the increasing likelihood as a function of time of particles becoming attached to the AFM tip apex, obscuring further images (imaging is always performed first on a large area, then zoomed in on a smaller region).

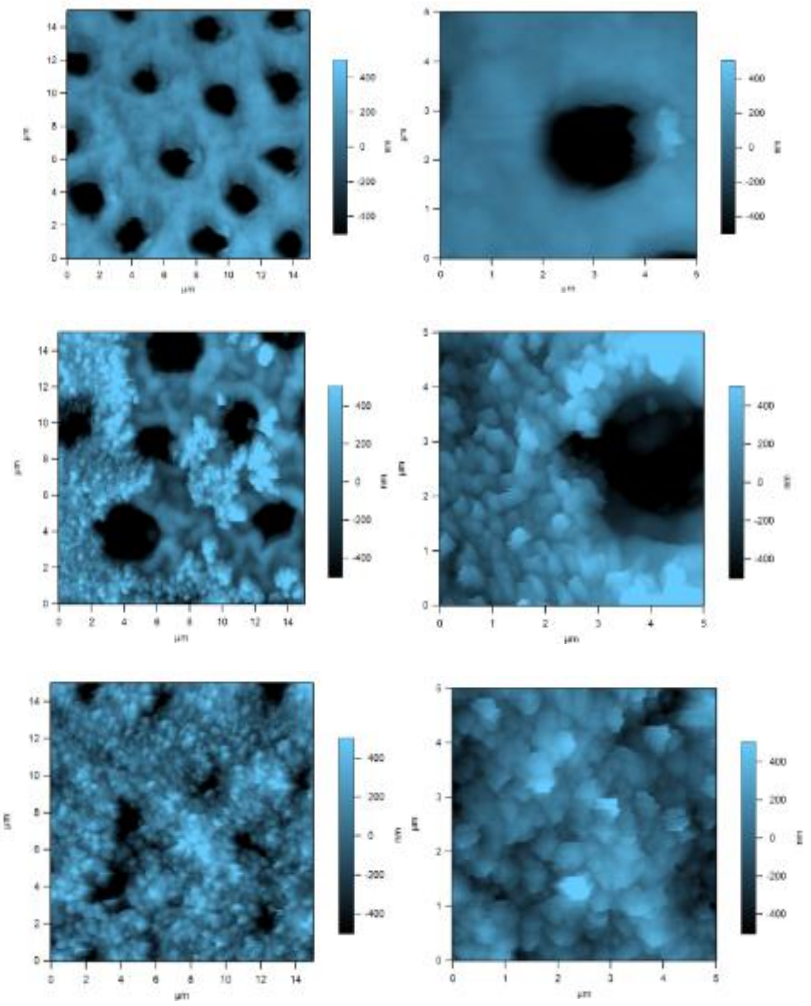

Figure 37. 15 um (left column) and 5 um (right column) topography images of coated (1st row) versus brushed and coated samples (rows 2 and 3)

In a final experiment in air, polymer was repeatedly deposited onto a bare tooth sample until 20 complete layers were built up, after initially preconditioning with DI water. In Figure 38, 15 um (left) and 5 um (right) height images of bare (top) and polymer coated (base) dentin and tubules are shown. In the 15 um image, the surface again becomes smoother upon polymer deposition. However, unlike for the previous figures, the holes were not spanned and it is unclear if they have been partially filled or not. In the 5 um image, it is easier to see that some holes were in fact partially filled around their edges

(and perhaps into their depth beyond the range of the AFM probe). Of course it is possible that the imaged features are remnants of a smear layer from the polishing preparation procedure, but such features were not seen elsewhere with bare teeth presumably due to their removal by the moderate acid etching step used on all specimens.

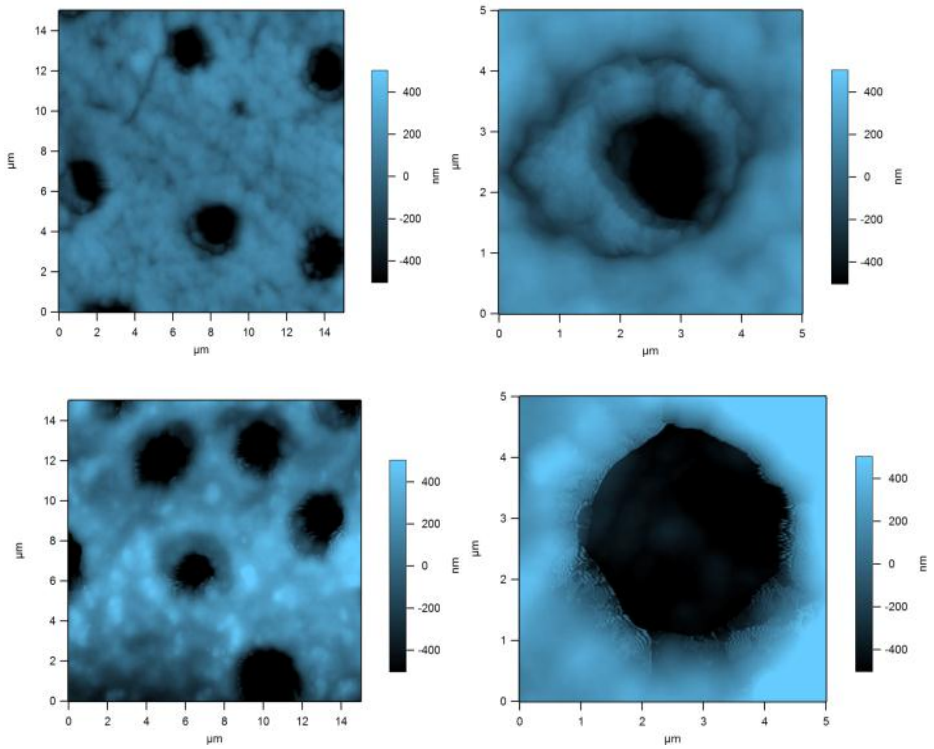

Figure 38. 15 um (left) and 5 um (right) topography images of bare (top) and 20 times polymer coated (base) dentin

4.2.5 Spin-Coated Dentin Substrate Rested at 37°C, Imaged in Air

The effect of elevated (body) temperature on the polymer deposition process and morphology was also considered. In Figure 39, 40 um (left), 15 um (middle) and 5 um (right) height (blue) and simultaneous phase (yellow) images are shown. The tubules are at least partially filled with polymer in every case, supported by the nearly uniform phase

contrast over the dentin and the spanned tubules themselves, indicative of homogeneous coverage of the otherwise topographically heterogeneous surface.

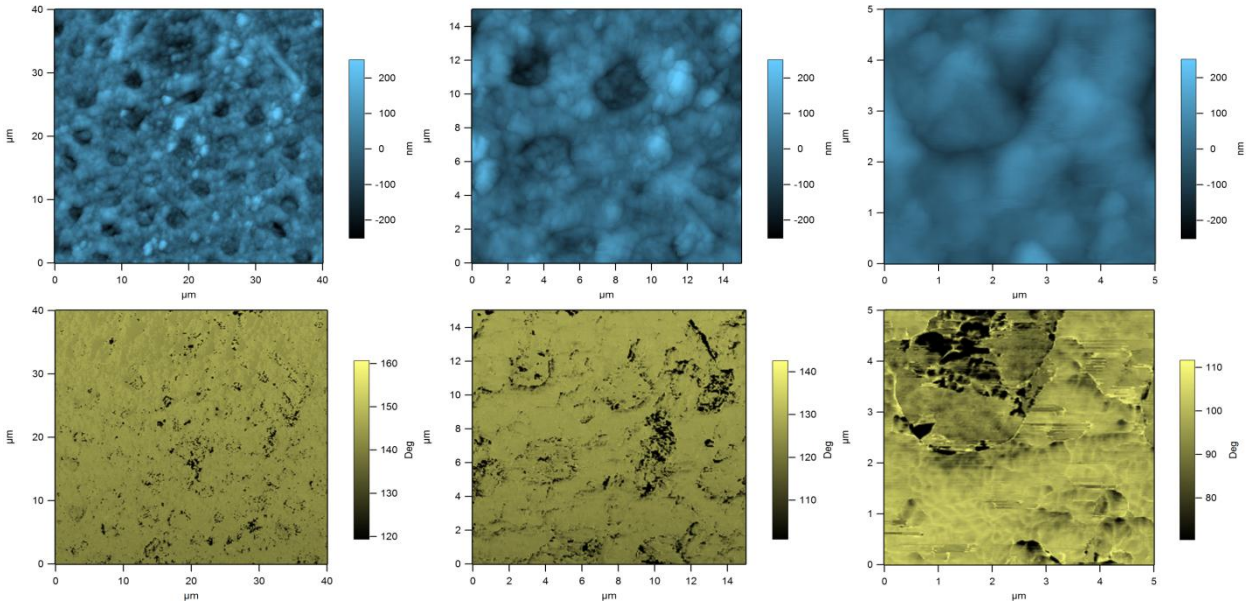

Figure 39. 40 um (left), 15 um (middle) and 5 um (right) topography (blue) and simultaneous phase (yellow) images of spin coated sample at 37 ˚C

4.3 In vitro imaging

Finally, measurements were performed in water to more closely relate the results to the in vivo conditions of teeth.

4.3.1 1 month Old, Spin-Coated Only - Dentin Substrate Imaged in Liquid

The first experiment of in-liquid AFM imaging was performed on a sample prepared by spin coating with 20 polymer layers, and then rested in air for 30 days. Figure 40 shows 10 um (left) and 3 um (right) height images of the sample acquired in DI water. Cracks

were observed on these images, most likely indicating drying of the polymer layer during the incubation period, followed by re-hydration during the experiment. The images indicate a remarkably smooth surface compared to the previous figures. Notably, the images are stable over time, indicating that the polymer coating is not appreciably dissolving in DI water during the experiment.

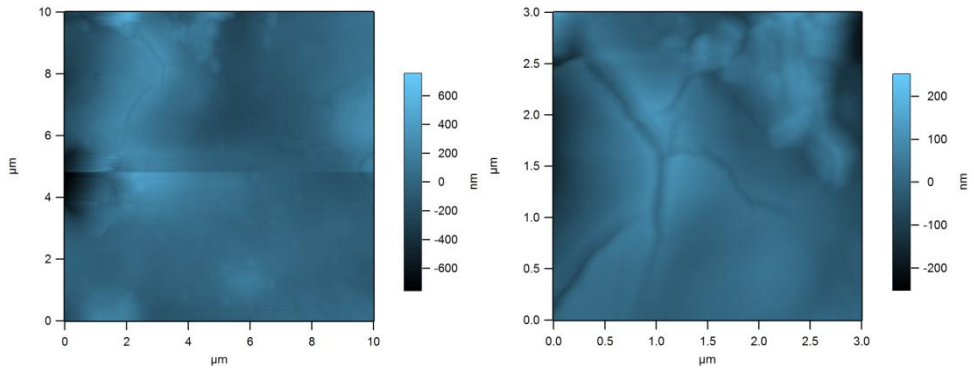

Figure 40. 10 um (left) and 3 um (right) height images of the sample acquired in DI water

4.3.2 Spin-Coated Dentin Substrate Imaged in Fluid with iDrive

At last, high resolution images were performed on the teeth and polymer specimens using a new hardware addition to the nmLabs, "iDrive." This system, designed for fluid imaging of fragile specimens such as biological materials, substantially simplifies and improves fluid imaging.

In the series of 40 um height images shown in Figure 41, changes caused by successive spin coatings are investigated with "iDrive" operated in deionized water. Although images are from different areas of the same tooth, they are sufficiently representative.

Bridging of the tubules by the polymer solution is rarely seen; however existence of clusters of material becomes readily apparent on the 8 and 10 times coated images (labels at lower left of each frame). These piles clearly cover the underlying tubules, and do not dissolve or disintegrate in the *in vitro* conditions implemented here (deionized water). Of course saline and protein-containing fluid is more biologically relevant for studies of teeth, but corresponding depositions of salt crystals and/or protein layers substantially complicate image analysis and thus were not implemented here.

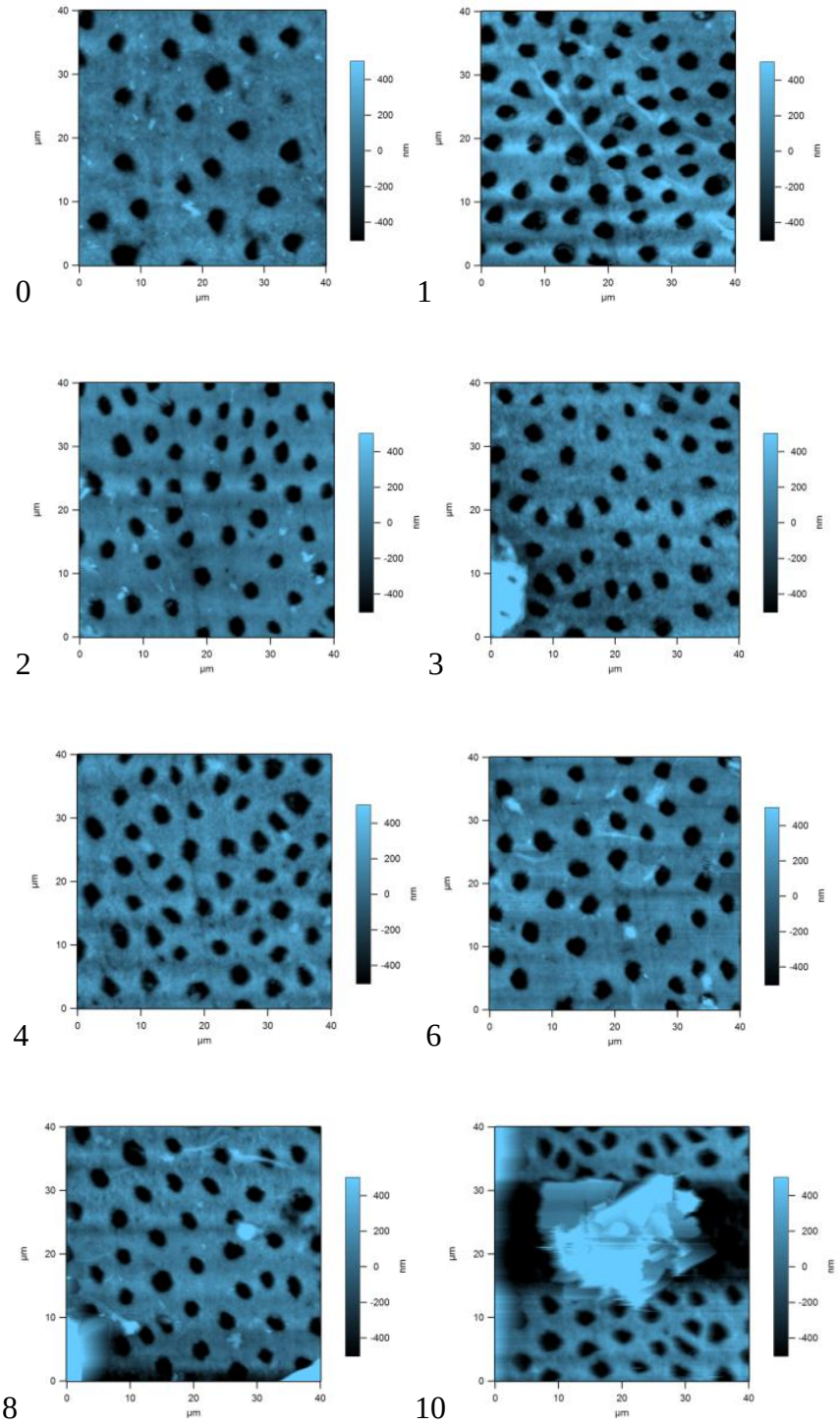

Figure 41. 40 um Height images of spin coated tooth substrate; layers increasing from left to right and top to bottom, "0" being bare tooth and "10" being 10 times spin coated tooth.

In Figure 42, zoomed in images for the same sample are shown. Tubule bridging is again rare, while large clusters of polymeric material again occur in some of the images. The first image labeled as “0” shows the bare dentin morphology where it is possible to see the underlying fibril texture. As the coating number increases, however, the fibril texture appears to disappear and lumps of material build up blocking the tubules.

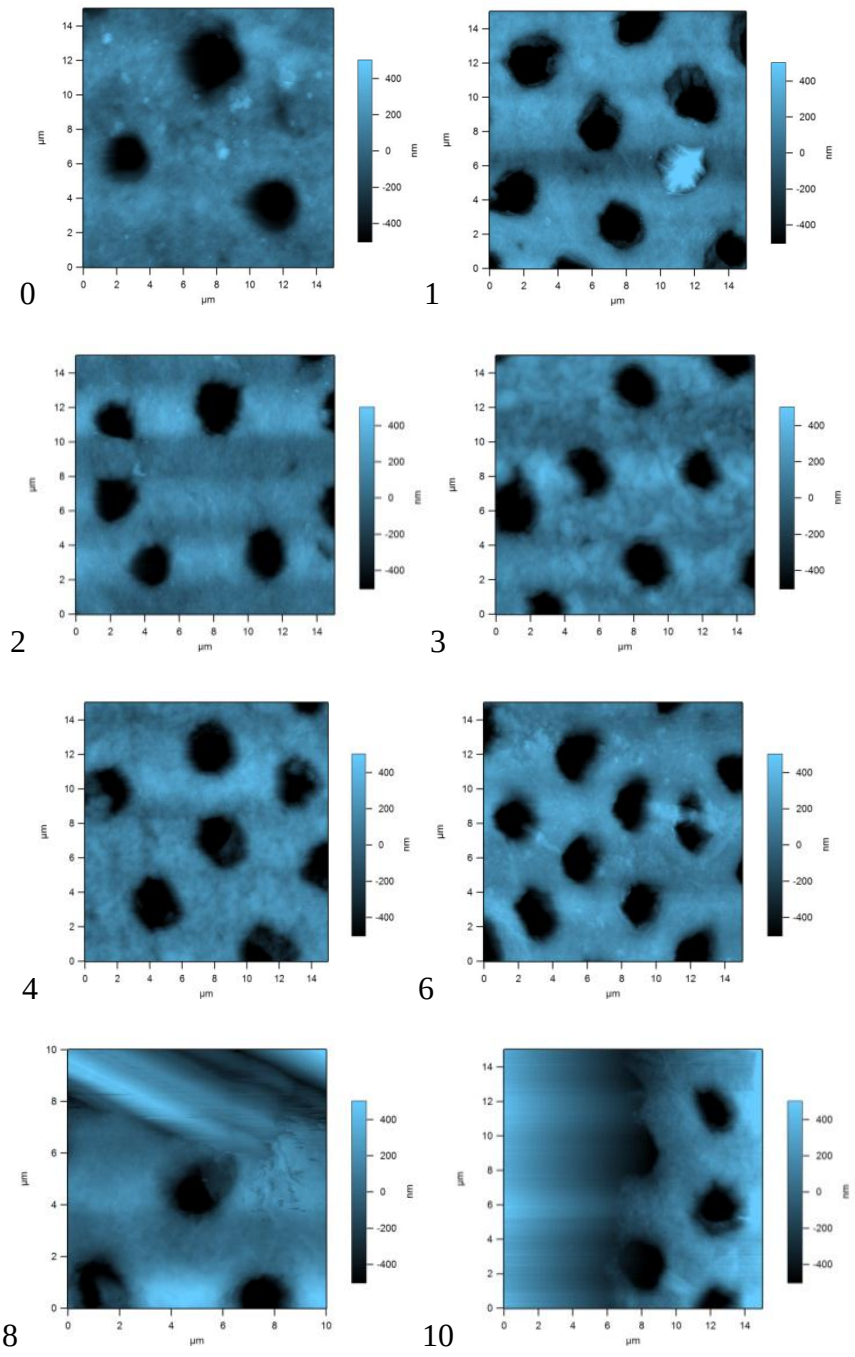

Figure 42. 15 um Height images of spin coated tooth substrate; layers increasing from left to right and top to bottom, "0" being bare tooth and "10" being 10 times spin coated tooth.

Figure 43 shows the largest scan area possible (80 um)^2 for the 10 times coated sample. Since the sizes of the particle clusters are several to even hundreds of microns, it was only possible to show image a few such structures in a single image.

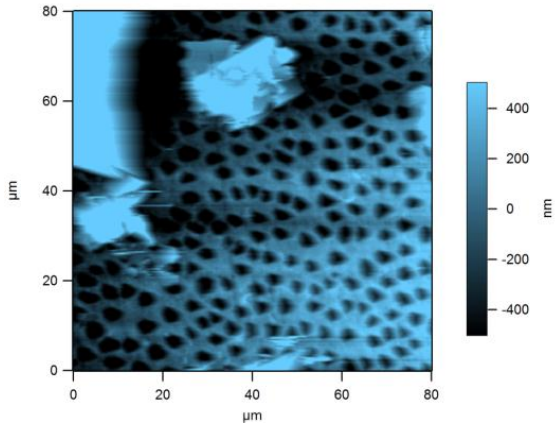

Figure 43. 80 um Height image of 10 times spin coated tooth sample

4.4 Experimental Challenges

The major experimental challenges for dentin experiments were the dense distribution of large and deep holes (tubules), the adhesive nature of the polymer solution, and challenges with liquid AFM imaging.

Especially while doing large area scans, for instance 40 um^2 - 80 um^2 on a side, the tip encounters many deep holes (tubules) which are always a challenge with AFM. The tip usually goes into a tubule with no difficulty; however when it is trying to climb out of the tubule during scanning, it can be caught by an overhanging edge, severely damping the lever amplitude, and hence making the AFM believe the tip is harshly contacting the surface. As a result, the z z-piezo retracts the tip as rapidly and as far as possible, causing

the height signal to overshoot the actual surface with a constant but often inaccurate slope. Artificial triangular shapes often result on the height cross sectional data. This is clearly revealed in Figure 44, which shows trace-direction cross sections of height and amplitude signals. The inaccurate surface representation caused by this behavior, highlighted by the superimposed dotted green line, is best overcome by slower scanning, with a corresponding loss of experimental efficiency.

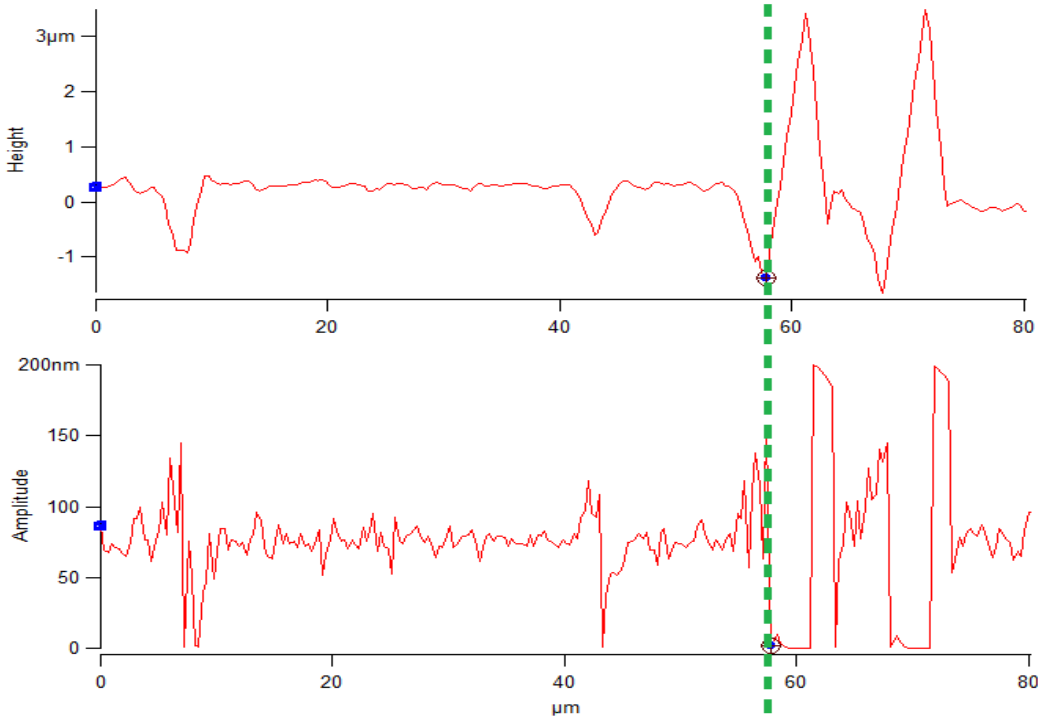

Figure 44. Cross sections of height trace (top) and amplitude trace (bottom) images of an 80 um^2 scan. Green dotted line shows the correspondence of amplitude behavior and height output

The adhesive nature of the polymer solution coated onto the dentin discs was another challenge as it often resulted in contaminating the AFM tips. In order to avoid this kind of contamination, the samples could be much more reliably imaged in air after a certain period of drying, again slowing down the experimental procedure. In fact, air imaging nearly required drying of the otherwise extraordinarily tacky polymer layers.

Another challenge occurred while imaging in fluid. The dentin discs were fixed on the coverslips by using superglue. It was observed that after spending a certain amount of time under water, the superglue began to detach from the coverslip. It was thought that a thin film of water makes its way in between the coverslip and glue layer, almost certainly through the tubules in the specimen since similar behavior is seldom seen with solid samples mounted in the same manner.

The final major challenge with these samples is that they were very prone to producing bubbles prior to and during fluid imaging. Since the dentin discs have tubules which are open to air on both faces of the specimen, when the sample was put in the fluid chamber of the AFM, it produces bubbles on the top surface of the disc. These bubbles make engaging on the surface very difficult, often impossible. In order to avoid this situation, the experimenter should wait until the bubbles form and then remove them by lightly tapping on the edge of the specimen. The agitation given by this tapping motion is usually enough to release the bubbles.

4.5 Future Work

A number of interesting studies could be conducted on dentin discs in the future. The most important would be performing Force – distance (F-d) measurements on bare and coated dentin surfaces. Relative stiffness values of both kinds of surfaces could be determined this way. Similarly, the adhesion properties of the polymer solution to the dentin itself could be identified by dipping the AFM tip into this solution and then applying F-d measurements on the bare dentin surface. A similar solution that lacks the polymeric component which gives the adhesive character could also be prepared and F-d measurements using this solution could be performed in order to serve as a.

Finally, the dentin discs could be sliced perpendicularly to the provided geometry in order to perform AFM measurements on a tubule lumen. The properties of the tubule lumen would be of interest to the researcher as the restorative agents could be observed as they build up on the walls of the tubule, resulting in coalescence leading to occlusion of the tubules.

Chapter 5: Summary and Future Work

5.1 Summary

In this work, nanocharacterization of porous materials is studied by in-air and in-liquid AC mode AFM imaging. This allows collecting height and phase contrast data by barely touching the surface, avoiding damage to the probe and/or the sample. Also, in-liquid imaging of biological samples provides a realistic in-situ environment successfully mimicking the actual physiological conditions. Porous samples from two distinct classes of materials are studied in this way; namely phosphoric acid fuel cell catalyst layers, and human molar dentin.

Fuel cell electrode catalyst layers with and without phosphoric acid (PA) impregnation are imaged in-air in order to investigate the morphology of the surfaces and the effect of PA impregnation on PTFE coatings. Results indicate that catalyst particles less than 100nm in diameter are resolvable with AFM. The PTFE coating seems to cover the catalytic particles, though unevenly. PTFE separation from catalytic particles has also been detected in the cathode. PA loaded samples seem to show significantly higher phase contrast, and even separation of the Teflon coating from the underlying catalyst. Also, while variations in the particle, coating, and impregnation morphology were expected based on preliminary SEM evidence supplied by the project collaborators, in fact only minor variations were observed from location to location with AFM. From a manufacturing point of view this is promising if it is an accurate representation of the specimens provided, though it may simply indicate that pockets of different morphologies develop during fuel cell manufacturing or use, yet these simply were not found during

this preliminary study. The small field of view of AFM, and necessarily slow imaging time for the samples of interest, therefore limits the use of this tool for quality control studies.

Dentin samples extracted from human molars are subjected to a polymeric solution and imaged both in-air and in-liquid. The results of treated and untreated surfaces are compared in terms of surface morphology. As expected the dentin and collagen are coated by the polymer with subsequent spin coating layers. This progression was monitored as a function of deposition layers, and a function of time, to monitor the surface development. In some cases, the polymer is also observed to partially span tubules (with a ratio of one or two out of 40). Although challenging, such AFM imaging in liquid provides a particularly good way to study biological materials like dentin since the environmental conditions are more realistic, simulating the human mouth.

5.2 Future Work

Future work building upon this preliminary effort can include a number of related studies, both on fuel cell catalyst layers as well as human dentin layers.

For PAFC electrode catalyst layers, efforts on targeted specimens which are expected to exhibit morphology variations in the particle, coating, and impregnation morphology based on preliminary SEM evidence supplied by the project collaborators would be interesting. This would allow the distribution of the microscale and nanoscale structure of the various components to be truly understood, whereas in the present work representative regions from convenient instead of targeted specimens were studied. In-

situ measurements of current conduction and especially heterogeneities in a working fuel cell could be studied as well.

For human dentin specimens, performing Force – distance (F-d) measurements on bare and coated dentin surfaces would be revealing in terms of the mechanical properties of the coatings. Adhesion properties of the polymer to the dentin could also be investigated by performing F-d measurements on bare dentin surfaces with polymer-functionalized AFM tips. A placebo solution prepared without the adhesive component in the polymer should also be considered to assess the efficacy of the engineered adhesion.

Finally, samples prepared with a different geometry designed to expose the tubule lumen could be assessed. The properties of the tubule lumen would be of interest to the researcher as the restorative agents could build up on the walls of the tubule, resulting in coalescence leading to occlusion of the tubules. There are many interesting academic questions about the mechanical and morphological properties of this lumen as well which such studies may reveal.

References

1. Antolini, E., (2003).*Formation, microstructural characteristics and stability of carbon supported platinum catalysts for low temperature fuel cells.* Journal of Materials Science. **38**(14): p. 2995-3005.

2. Kangasniemi, K.H., D.A. Condit, and T.D. Jarvi, (2004).*Characterization of Vulcan Electrochemically Oxidized under Simulated PEM Fuel Cell Conditions.* Journal of The Electrochemical Society. **151**(4): p. E125-E132.

3. A., G., (1900).*An attempt to explain the sensitiveness of dentin.* Br J Dent Sci. **43**: p. 865-868.

4. Sergei N. Magonov, M.-H.W., (1996).*Surface Analysis with STM and AFM Experimetal and Theoretical Aspects of Image Analysis*. Tokyo: VCH.

5. J.I. Paredes, A.M.-A., J.M.D. Tascon, *Scanning probe microscopies for the characterization of porous solids: strengths and limitations*, in *Characterization of Porous Solids VI, Proceedings of the 6th International Symposium on the Characterization of Porous Solids, Alicante, Spain*, B.M. F. Rodriguez-Reinoso, J. Rouquerol and K. Unger, Editor. 2002, Elsevier.

6. Brasquet, C. and P. Le Cloirec, (1999).*Effects of Activated Carbon Cloth Surface on Organic Adsorption in Aqueous Solutions. Use of Statistical Methods To Describe Mechanisms†.* Langmuir. **15**(18): p. 5906-5912.

7. Brasquet, C., et al., (2000).*Observation of activated carbon fibres with SEM and AFM correlation with adsorption data in aqueous solution.* Carbon. **38**(3): p. 407-422.

8. Curran, M.D., D.D. Pooré, and A.E. Stiegman, (1998).*Vanadia−Silica Sol−Gel Derived Glass: Factors Affecting Homogeneity and Morphology.* Chemistry of Materials. **10**(10): p. 3156-3166.

9. Richard Bowen, W., et al., (1996).*Atomic force microscope studies of membranes: Surface pore structures of Cyclopore and Anopore membranes.* Journal of Membrane Science. **110**(2): p. 233-238.

10. Bailey, D.A., et al., (2000).*Characterization of alumoxane-derived ceramic membranes.* Journal of Membrane Science. **176**(1): p. 1-9.

11. Stamatialis, D.F., C.R. Dias, and M.N. de Pinho, (2000).*Structure and Permeation Properties of Cellulose Esters Asymmetric Membranes.* Biomacromolecules. **1**(4): p. 564-570.

12. Hennesthal, C. and C. Steinem, (2000).*Pore-Spanning Lipid Bilayers Visualized by Scanning Force Microscopy.* Journal of the American Chemical Society. **122**(33): p. 8085-8086.

13. Zapletalova, Z., et al., (2004).*Examination of dentin surface using AFM (our experience).* Acta Medica (Hradec Kralove). **47**(4): p. 343-6.

14. Appleby, A.J., (1989).*Fuel cell handbook / A.J. Appleby, F.R. Foulkes*, ed. F.R. Foulkes. New York :: Van Nostrand Reinhold.

15. Sammes, N., R. Bove, and K. Stahl, (2004).*Phosphoric acid fuel cells: Fundamentals and applications.* Current Opinion in Solid State and Materials Science. **8**(5): p. 372-378.

16. Shah, R., *Introduction to Fuel Cells*

Recent Trends in Fuel Cell Science and Technology, S. Basu, Editor. 2007, Springer New York. p. 1-9.

17. Choudhury, S., *Phosphoric Acid Fuel Cell Technology*

Recent Trends in Fuel Cell Science and Technology, S. Basu, Editor. 2007, Springer New York. p. 188-216.

18. Larminie, J. and A. Dicks, (1999).*Fuel Cell Systems Explained*. 2 ed.: John Wiley & Sons.

19. Kinoshita, K., (1988).*Carbon: Electrochemical and Physicochemical Properties*, New York: Wiley-Interscience.

20. Choi, B.-W., S.-J. Chung, and D.-R. Shin, (1996).*Microstructure of PTFE and acid absorption behavior in PTFE-bonded carbon electrodes.* International Journal of Hydrogen Energy. **21**(7): p. 541-546.

21. Kumar, P.S., (2004).*Dental Anatomy and Tooth Morphology*. New Delhi: Jaypee Brothers Medical Publishers Ltd.

22. Marshall, G.W., Jr., et al., (1997).*The dentin substrate: structure and properties related to bonding.* J Dent. **25**(6): p. 441-58.

23. F.C.M. Driessens, R.M.H.V., (1990).*Biominerals*. Boca Raton: CRC Press. 428.

24. Ten Cate, A.R., (1994).*Oral Histology: Development, Structure and Function*. Vol. 4. St Louis: Mosby.

25. Sharma, S., et al., (2010).*Nanocharacterization in dentistry.* Int J Mol Sci. **11**(6): p. 2523-45.

26. Silikas, N., et al., (1999).*Surface fine structure of treated dentine investigated with tapping mode atomic force microscopy (TMAFM).* J Dent. **27**(2): p. 137-44.

27. Bertassoni, L.E., et al., (2010).*Evaluation of surface structural and mechanical changes following remineralization of dentin.* Scanning. **32**(5): p. 312-9.

28. Wallace, J.M., et al., (2010).*Type I collagen exists as a distribution of nanoscale morphologies in teeth, bones, and tendons.* Langmuir. **26**(10): p. 7349-54.

29. Lo, C.-H.C.E.C.-M., (2010).*Dentin hypersensitivity: a review.* Hong Kong Dent J. **7**(1).

30. Dowell, P. and M. Addy, (1983).*Dentine hypersensitivity--a review. Aetiology, symptoms and theories of pain production.* J Clin Periodontol. **10**(4): p. 341-50.

31. M., B., (1962). *A hydrodynamic mechanism in the transmission of pain producing stimuli through the dentine.* Anderson D J. p. 73-79.

32. Berman, L.H., (1985).*Dentinal sensation and hypersensitivity. A review of mechanisms and treatment alternatives.* J Periodontol. **56**(4): p. 216-22.

33. PA, W., (2005).*Dentinal Hypersensitivity: A Review*. J Contemp Dent Pract **6**(2): p. 107-117.

34. Scherman, A. and P.L. Jacobsen, (1992).*Managing dentin hypersensitivity: what treatment to recommend to patients.* J Am Dent Assoc. **123**(4): p. 57-61.

35. A., G.L., (1935).*Systematic method for the treatment of hypersensitive dentine.* J Am Dent Assoc. **22**: p. 592-598.

36. Dababneh, R.H., A.T. Khouri, and M. Addy, (1999).*Dentine hypersensitivity - an enigma? A review of terminology, mechanisms, aetiology and management.* Br Dent J. **187**(11): p. 606-11; discussion 603.

37. Petrou, I., et al., (2009).*A breakthrough therapy for dentin hypersensitivity: how dental products containing 8% arginine and calcium carbonate work to deliver effective relief of sensitive teeth.* J Clin Dent. **20**(1): p. 23-31.

38. Brannstrom, M. and A. Astrom, (1972).*The hydrodynamics of the dentine; its possible relationship to dentinal pain.* Int Dent J. **22**(2): p. 219-27.

39. Holland, G.R., et al., (1997).*Guidelines for the design and conduct of clinical trials on dentine hypersensitivity.* J Clin Periodontol. **24**(11): p. 808-13.

40. Renton-Harper, P. and M. Midda, (1992).*NdYAG laser treatment of dentinal hypersensitivity.* British Dental Journal. **172**(13): p. 16.

41. Orchardson, R. and D.G. Gillam, (2006).*Managing dentin hypersensitivity.* J Am Dent Assoc. **137**(7): p. 990-8; quiz 1028-9.

42. Roman Kubinek, Z.Z., Milan Vujtek, Radko Novotný, Hana Kolarova and Hana Chmelickova, (2007).*Examination of dentin surface using AFM and SEM.* Modern Research and Educational Topics in Microscopy.

43. Choi, S., et al., (2010).*Effect of fluoride pretreatment on primary and permanent tooth surfaces by acid-etching.* Scanning. **32**(6): p. 375-82.

44. Binnig, G., C.F. Quate, and C. Gerber, (1986).*Atomic Force Microscope.* Physical Review Letters. **56**(9): p. 930-933.

45. Nicholas A, G., (2009).*AFM and combined optical techniques.* Materials Today. **12**(7–8): p. 40-45.